DESIGN OF ADVANCED HID HEADLAMP SYSTEM, AUTO LIGHT BEAM LEVEL CONTROL AND GLARING PREVENTION

CHAN CHIK KEE

M.Phil

The Hong Kong Polytechnic University

2009

The Hong Kong Polytechnic University

Department of Electrical Engineering

Design of Advanced HID Headlamp System, Auto Light Beam Level Control & Glaring Prevention

Chan Chik Kee

A thesis submitted in partial fulfilment

of the requirements for the Degree of

Master of Philosophy

August 2008

CERTIFICATION OF ORIGINALITY

I hereby declare that this thesis is my own work and that, to the best of my knowledge and belief, it reproduces no material previously published or written nor material which has been accepted for the award of any other degree or diploma, except where due acknowledgement has been made in text.

_____ (Signature)

CHAN Chik Kee (Name of Student)

Abstract

HID lamps on account of their high brightness and efficiency are being adopted as a replacement to the traditional Halogen lamps in automobile lighting systems. However, HID lamp produces more glares compared to Halogen lamps due to sharper cut-off point of its light pattern. The abrupt shift from the dark to bright region of its light pattern is known to cause glare to the oncoming vehicles resulting in temporary discomfort to the oncoming drivers. The present work is related to the solution to overcome the problem of glare caused by the use of HID lamps. Accordingly a system which can control the direction of the light beam from the HID lamp is developed in the current work. Power saving and high power efficiency are also the concerns for this project.

In the study of Advanced Headlamp Control System, two types of drive have been examined to control the headlamps that are stepper motor and servo motor. Comparison has been made for the performance and cost. It has been found that the stepper motor provide a higher performance in response time and robustness. Lower cost in overall system is also found. . The Adaptive Front Lighting System (AFS) control is highly related to the distance of the obstacle. Different distance will trigger different operations of the AFS. Simulation of the system by Matlab has been done to examine different cases and conditions. The logic, the input and output of the system have been simulated through software. A number of cases have been done to study the

operation condition in details.

In automotive system, the voltage conversion from the battery voltage to other unit is important. The present system is to develop a low EMI converter that converts battery voltage 12V to 6V for the control electronics of the proposed Advanced Headlamp Control System. A new switched-capacitor resonant converter is proposed that eliminates the level-shifted gate drive. A circulation inductor is inserted to reduce the shoot-through current. A formulation of the circuit is presented. The method can be extended to other voltage conversion system and other switched-capacitor topologies.

Finally, the implementation of the AFS to an electric vehicle is discussed. The design of the EV based on the total running resistance is to use design the motor drive system. The overall vehicle with the installation of the AFS is finally prototyped and demonstrated in an electric vehicle EV4.

Publications – Conference papers

Conference Papers

C.K.Chan, K.W.E.Cheng and S.L.Ho, “Development of Packaging and Electrical Interfacing for Electrical Vehicles”, *Proc. PESA ’06,* pp. 234 – 240. Nov 2006.

C.K.Chan, K.W.E.Cheng and S.L.Ho, “Simulation of the control method for the adaptive front lighting system”, *Proc. PESA ’09,* Accepted for publication.

C.K.Chan, K.W.E.Cheng, S.L.Ho and W.F.Choi, “Development of electric vehicle with advanced lighting system and all electric drive”, *Proc. PESA ’09,* Accepted for publication.

Journal paper

C.K.Chan, K.W.E.Cheng and S.L.Ho, “Half-bridge converter based on Switched-capacitor Resonance without Using Deadtime Control”, IET – Proc. Power Electronics, (Provisional Accepted)

Acknowledgements

I would like to express thanks to my parents and relatives for their continuous support. I would also like to give thanks to my supervisor, Professor Ka-wai Eric Cheng, for his continuing guidance and encouragement throughout the course of my studies. I would also like to thanks my Co-supervisor Professor Siu-lau Ho, and everyone in Power Electronics group of Department of Electrical Engineering. I also would like to thank everyone in my department.

A special thank goes to Mr. William Choi, Dr. B.P. Divakar, Ms. Ann Xu, Dr. Benny Yeung, and Mr. James Ho for their great technical support and guidance. I would thank Mr. Peter Fung, Mr. Stanley Tsui, Mr. Leo Wong, Mr. Johnson Lau and all my friends for their support.

Table of Content

List of Figures

List of Tables

List of Key Symbols

l_1	-	Ultrasonic Sensor Long Range Distance (m)
l_1	-	Ultrasonic Sensor Short Range Distance (m)
S_u	-	Light Sensor (Upwards)
S_d	-	Light Sensor (Forward)
θ	-	Headlamp Angle from Horizontal (rad)
v	-	Voltage (V)
h	-	Height of headlamp from ground (m)
h_2	-	Rear Suspension Height (m)
h_1	-	Front Suspension Height (m)
l	-	Wheelbase of vehicle (m)
k_{uL}	-	a coefficient of the ultrasonic sensor
u_x	-	Ultrasonic Sensor
u_1	-	High beam
u_2	-	Low Beam.
L_{12}	-	inductance of tapped inductor (H)
V_{GD}	-	Supply voltage to self-driven gate-drive (V)
Z	-	Resonant impedance (Ω)
ω_o	-	Resonant frequency (rad/s)

V_{in}	-	Input voltage (V)
i_{Lr}	-	Resonant inductor current (A)
V_{C1}	-	Switched capacitor voltage (V)
I_o	-	Output current (A)
I_{in}	-	Input current (A)
T_{ov}	-	Overlapped time (s)
T_r	-	Resonant period (s)
τ	-	Torque (Nm)
I_{12}	-	Boundary current between State I and State II for i_{Lr}
F	-	Motive Force (kg/h)
M	-	Motor Torque (Nm)
i	-	Transmission Ratio
η	-	Drivetrain efficiency
r	-	Wheel radius (m)
F_{st}	-	Climbing Resistance (kW)
g	-	Weight (N)
m	-	Vehicle mass (kg)
g	-	Gravitational Acceleration ($9.81 m/s^2$)
v	-	Vehicle Speed (m/s)
α	-	Gradient Angle (rad)
F_D	-	Aerodynamic Drag (N)

ρ	-	Air Density (kg/m^3)
C_d	-	Coefficient of Drag (N/m^2)
A	-	Largest Cross Section of the Vehicle (m^2)
v_o	-	Headwind Speed (m/s)
F_{Ro}	-	Aerodynamic Drag
f	-	Coefficient of Rolling resistance
F_W	-	Running Resistance (N)
F_L	-	Aerodynamic Drag (N)
F_{st}	-	Climbing Resistance (N)
P_W	-	Running Power Resistance (kW)

Acronym

AFS	-	Adaptive Front Lighting System
AAFS	-	Advanced Adaptive Front lamp System
HID	-	High Intensity Discharge
ESP	-	Electronic Stability Programme
ACC	-	Adaptive Cruise Control

Chapter 1. Background of Research

1.1 Introduction

Headlamp is one of the crucial safety elements of vehicle accessory. The headlamp lighting system generally contains two lighting modes namely, High-beam and Low-beam. In High-beam mode, the light is projected far ahead while the light is projected with a dipped angle so as not to cause glare in Low-beam position. The High-beam mode is used for high speed driving in areas with poor visibility or requires maximum visibility whereas Low-beam mode is used in low speed driving under normal visible conditions. Headlamp assembly in automobiles serves two major functions: a) housing the headlamp b) projecting the light with a standard pattern by the reflectors so as not to cause glare.

Figure 1.1 Old Headlamp fuelled by acetylene

The first headlamp was invented in 1880. At that moment, the headlamp was fuelled by acetylene or oil. The first electric powered headlamp was invented in 1908. The design of headlamp was very simple. There were no specifically designed reflector and lens. There

was only one concave mirror with a glass mounted at the front. In late 1920s, number of cars grows dramatically. Regulations of vehicle started established in many countries. Headlamp becomes one of the components which were guided by the new law because it is directly related to road safety. The new regulations included the aim of the light beam and the brightness.

Figure 1.2: Headlamp with glass magnifier (Corning Conaphore headlamp)

At that time, newly designed headlamp had the features of High/Low beam and magnified glass cover for focusing the light beam. The name of this headlamp was Corning Conaphore headlamp.

Low beam headlamps were introduced in 1920s. The first modern unit having the light for both low (dipped) and high (main) beams of a headlamp emitting from a single bulb was invented in 1924. The first halogen headlamp for vehicle use was introduced in 1962. Halogen technology makes incandescent filaments more efficient and can produce 50% more light than from non-halogen filaments at the same power consumption. Dual filament halogen lamp was introduced in the 1970s and still widely used nowadays on those low priced cars. High-intensity discharge (HID) systems were introduced in 1991's. HID lamp produced 2.7 times

more than standard halogen bulbs. Therefore recently there was numerous research has reported on the electronic ballast of HID lamps [1-8]. European and Japanese markets began to prefer HID headlamps because of its better brightness and efficiency [9-11]. Advanced version of HID ballast has also been reported [12-15]. The brightness of headlamps is also related to road safely as well.

Figure 1.3a: Alfa Romeo Halogen

Figure 1.3b: Alfa Romeo HID Headlamp.

In some recent researches about road safety, old drivers generally cause traffic accident because of the decline of their capabilities. Eyes change with age. They lose focus quickly. Retina becomes less sensitive to light. They would try to avoid busy roads or night time driving in order to reduce risks. In the findings, we found that a 20-year-old youngster needs 1.5 times more light than a 10 year old child to do the same task and a 60 elderly needs 11 times the amount to light as a 10 year old child to do the same task. Generally, the driver fails to see the hazard and stop in time is the main cause of most of the accidents that occur at the night time.

As a result, the elderly behind the wheels should have a brighter headlamp that projects light over a long distance.

1.2 Glaring

Glaring is the discomfort or blindness caused by showering of unwanted lights temporarily. The main reason behind the glare is due to shifting of the light beam when a vehicle moves over uneven surfaces. The simple head lighting systems without any self beam correcting features are unable to maintain the light beam with respect to the suspension ride height of the vehicle that is the prime source of glare. According to consumer reports in US, HID produces more glare than halogen lamps. The reason is that the cut-off point of HID lamp is very sharp and crisp comparing with halogen lamp and there is a sudden shift from dark to bright region, unlike halogen lamp which show some overlapping. Although the earlier system with Halogen lamps were producing glares, the problem was not perceived as a serious threat to the safety of the oncoming drivers until the use of HID lamps that are brighter than Halogen lamps. The glare can be minimized by automatically controlling the level of the light beam with reference to some external inputs such as suspension ride heights, speed and distance between the vehicles. A system that processes useful external information in maintaining the level of light beam under different road conditions is the subject of the present study.

1.3 Literature Review

Several research papers related to this project have been studied. Two chosen papers Reference [16] & [17] are reviewed in the following. The group of T.Hacibekir and S.Karaman published a paper on Adaptive Headlight System Design Using Hardware-In-The-Loop Simulation [16]. It proposed an adaptive headlight system adjusting headlight horizontal angle automatically according to the radius of curvature of vehicles calculated from a mathematical model. This paper points out that most road accidents occur at night so that improving visual conditions of vehicle drivers by adjusting highlight angles is concerned. A mathematical model for calculating the radius of curvature of a car is shown in this paper. This model includes a simple model of engine, tire conditions and slip conditions. A controller of this system is proposed too. It calculates the radius of curvature with the model and controls the horizontal angle of the headlight in normal condition, and reset the headlight to be default angle in emergency and slip condition. Simulation method and results with different vehicle conditions are obtained and explained.

The group of J.Roslak, L-LAB, and J. Wallaschek, published a paper on Active Lighting Systems for Improved Road Safety [17]. It introduced some more methods improving road safety with headlight systems of vehicles. First of all, this paper suggested avoiding glare effect by adjusting vertical angle of headlight beam. This system can also warn the driver early of potential dangers on the road. This paper also introduced a system similar to the system that the previous paper proposed. This system receives information such as the signals from steering angle sensors, ESP (Electronic Stability Programme), yaw rate sensors, and ACC (Adaptive Cruise Control). It analyses the information to control the horizontal angle of headlight automatically. This paper also suggested a system of headlight changing headlight beam pattern which can be used in the future. Changing headlight beam pattern can be achieved by novel optical concepts for the generation of predefined beam patterns, such as pixel light or active optical elements. Micro mirror devices (DMD-chip) are applied in these headlamps. The light beam generated by a light source is deflected by these tiny mirrors and projected in one of two directions, onto the road surface in the on-state and into the absorber in the off-state. Each generated pixel is controlled by a control unit. This paper pointed out that headlamp control strategy is very important as well. In this literature, some important issues and information have been suggested such as sensor signals and human behaviours.

1.4 High Intensity Discharge Lamps

High Intensity Discharge (HID) lamps are widely used in vehicles in recent years. Due to the advantages of high lumen/watt ratio, better colour temperature and longer life, it becomes widely accepted by customers and becoming a standard equipment of new cars. HID lamps deliver high output compared to halogen lamps but with relatively low consumption of power. They are operated at 70W during start up to meet SAE J2009 standard and 35W at steady state. They are being fitted in high beam, low beam and both, and operated at the same rated power of 35W for both high and low-beam fittings.

1.5 Automatic High/Low Beam System

Automatic High/Low Beam System firstly existed in 1952 by General Motor called “Autronic Eye”. It was a device on automobiles which used a photoresistor to automatically adjust the headlight beams from "High beam" to "Low beam" when encountering oncoming vehicles during night time driving, and to switch back to high beam after the vehicles had passed. A periscope-like phototube that sat on the dashboard's left side inside the windshield was the location of the photoresistor.

Drivers could also use standard headlight dimmers (such as foot-operated

devices) to override the automatic headlight dimmer on cars so equipped.

One criticism of early automatic headlight dimmers was that the headlights tended to erratically flicker between low- and high-beams in response to minor fluctuations of light, such as street lamps.

GM discarded Autronic Eye after 1958 and launched an improved version of automatic headlight dimming system called GuideMatic in 1959. The GuideMatic had a switch that allowed drivers to adjust when the headlights dimmed. Though the GuideMatic system was an improvement over the Autronic Eye, many GM customers were leery through past experience and feared that the new system was still too erratic. GuideMatic was finally dropped on all GM models by mid-1960s.

1.6 Self-levelling Control System

Self-levelling Control System controls headlamp beam angles according to the pitch of a vehicle. The pitch of the vehicle changes during acceleration, deceleration and payload changes. Starting from year 1990 required by the ECE Regulations, all vehicles equipped with headlamps brighter than 2000 lumens (such as HID Headlamp) must be equipped with a self levelling control. This can ensure the beams aimed correctly. The first car in the world equipped with Self-Levelling

Control System was a French manufacturer, Panhard Dyna Z, in 1954. Their headlamp was mechanically linked to a suspension arm in which the headlamp was constantly adjusted relative to the position of the suspension arm. This linking of the headlamp to the suspension arm resulted in the automatic levelling control of light beam. The system did not last for many years. The reason was lack of interest of buyers due to high cost of production. Also, the system mechanism was very complicated.

Beginning in the 1970s, some other European countries like Germany began requiring remote-control headlamp levelling systems that permit drivers to alter the beam position by means of a lever or a knob located close to the dashboard of the vehicle. This mechanism allows drivers to adjust the position of the beam with reference to the shift in the rear side of the vehicle due to the load from passengers or cargo. Such systems typically use stepper motors at the headlamp and a rotary switch on the dash marked "0", "1", "2", "3" for different beam heights, "0" being the "normal" (and highest) position when the car is lightly loaded and “3” being the lowest position when the car is fully loaded. This mechanism is not satisfactory as it is manual and most drivers seems ignoring it.

In the 1990s, some cars were equipped with an automatic levelling device which controlled the beam aimed position according to the outputs of two

hall-effect sensors mounted on the vehicle chassis linked with the suspension arms. The sensors record the movement of the suspension arm and output signals proportional to the pitch angle the vehicle. A processor then calculates the new position of the headlamp based on the outputs of the two sensors. Thus the angle of the headlamp reflector lens is adjusted via the stepper motor mounted on the headlamp housing.

The major working principle is as follows:

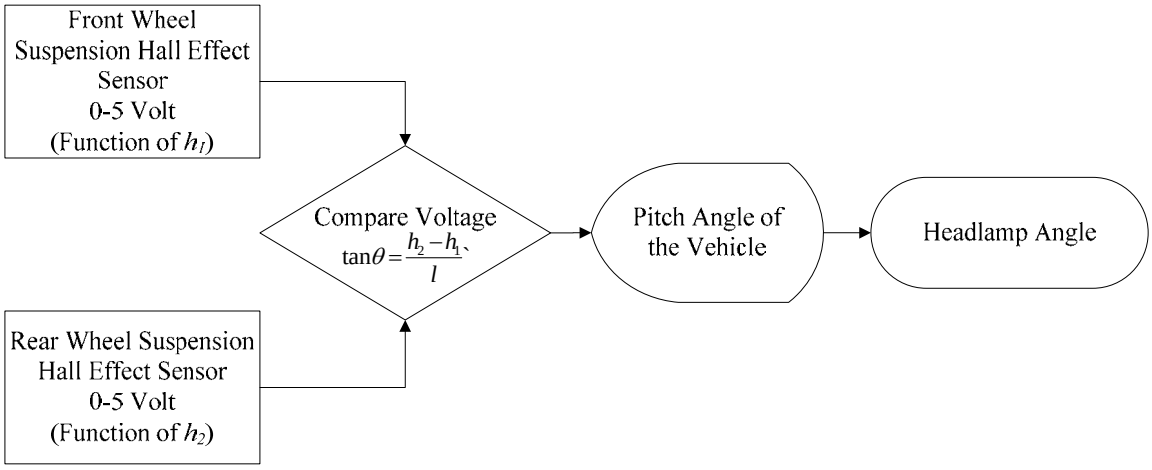

Figure 1.4: Principle of self levelling system in the market

Since it is only an open-loop system, the judgment of headlamp beam angle only calculates based on the relative angle of the vehicle instead of the absolute angle. Therefore, a system which can also monitor the other measurement beside the vehicle must be developed in order to properly aim the light beam.

1.7 Light Dimming Control

The main purpose of any head lighting system is to provide adequate visibility to drivers under poor visible conditions. Halogen lamps consume 55 W and produce about 1200 Lumens while an HID lamp consumes 35 W and produces 2500 Lumens of light output. Although high brightness of lamps is desirable in low visibility conditions, it becomes less important on roads that are very well lit as in modern cities around the world. In addition, due to high density of vehicles in cities around the world there is a possibility of slow moving traffic or frequent traffic jams leading to lining of vehicles one behind the other. The driver of a vehicle may experience glare due to reflection of the car's light off the surface of the car in front and may have to turn off the headlight to avoid discomfort.

So, it can be concluded that brightness of the lamps is not vital for driving on roads with good visibility and where traffic density is high. Therefore there is a provision for dimming the HID lamp with a view to saving the energy but without sacrificing the safety under such road conditions.

1.8 Adaptive Front Lighting System

Adaptive Front Lighting System is the combination of Automatic Self Levelling control system and the Angle Adjustable Headlamp module. The Angle

of the headlamp will be change according to the steering wheel angle sensed by the steering angle sensor located behind the steering wheel. This minimized the blind spot from the headlamp during the vehicle corners.

1.9 Summary

In this chapter, a background of head light for vehicle has been described. A literature survey on the HID lamps has been conducted.. The effect of glaring due to headlight is discussed. The chapter also introduces the automatic high and low beam requirement for vehicle. The self-level control and dimming control are explained. The chapter also provides a brief history of the head lamps and how the car manufacturers have progressed in the last 80 years.

Chapter 2.Principle of Operation

2.1 Introduction

The control of headlamp consists of two major parts. The first part is the compensation of vehicle pitch to the headlamp. The second part is the control of light beam projection angle in the headlamp. Since the pitch detecting control is well developed and widely used nowadays. No major improvement can be done on the first part. We will mainly focus on the second part.

How vehicle pitch affecting headlamp angle:

Figure 2.1: Vehicles sit horizontally – Light beams

In Figure 2.1, since the headlamp is adjusted according to the horizontal level. The headlamp focuses positions correctly.

Figure 2.2 Vehicles pitch up – Light Beams

In Figure 2.2, when the vehicle accelerates or heavy loaded at the rear of the

vehicle, the vehicle will start pitching up. The lamp housing will be pitching up together with the vehicle therefore the focus of the headlamp will go up and higher than the target.

Figure 2.3 Vehicles pitch down – Light Beams

In Figure 2.3, when the vehicle decelerates, the vehicle will pitch down. The projected area of light will be closer since the angle of headlamp decreases.

The pitch of vehicle changes during acceleration, deceleration and payload varies. Since the headlamp housing is fixed in the vehicle chassis, load sensors have been installed on both front and rear suspension arms. The value feedback from the load sensor can show the pitch angle of the vehicle and compensate the value in the headlamp assembly.

An advanced headlamp system is proposed in this thesis. This new system consists of three major parts. The first part is Automatic High/Low (Hi/Lo) Beam System. The second part is Low Beam Adjustment System. The third part is HID Dimming System. These three systems are working individually on different stages.

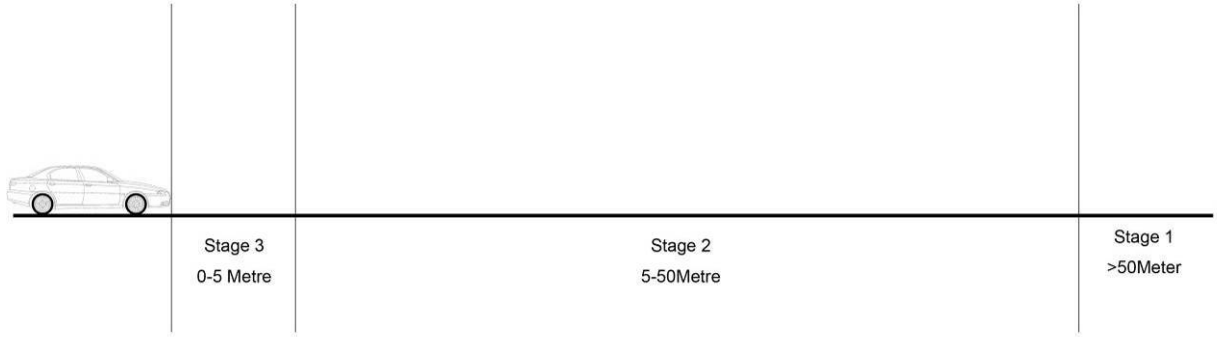

Figure 2.4: Stages of Advanced Headlamp System

Figure 2.4 shows that there are 3 stages in the system. The first stage represents the range of the nearest obstacles over 50 metres ahead. The second stage represents the obstacles within 5-50metres range and finally the third stage represents the obstacles with 0 - 5metres ahead.

When the system detects an object which is very far away, Automatic Hi/Lo beam system will operates. (Stage 1, Figure 2.5) When the obstacles go closer (stage 2, Figure 2.6), the headlamp control will operate. Finally, when the obstacles or cars are very close (Stage 3, Figure 2.7); HID Dimming System for low beam will take into control. An adjustment will be carried out the angle of headlamp as compensation to the pitch angle of the vehicle.

In this case, assuming the pitch of the vehicle is fixed in horizontal position and constant velocity.

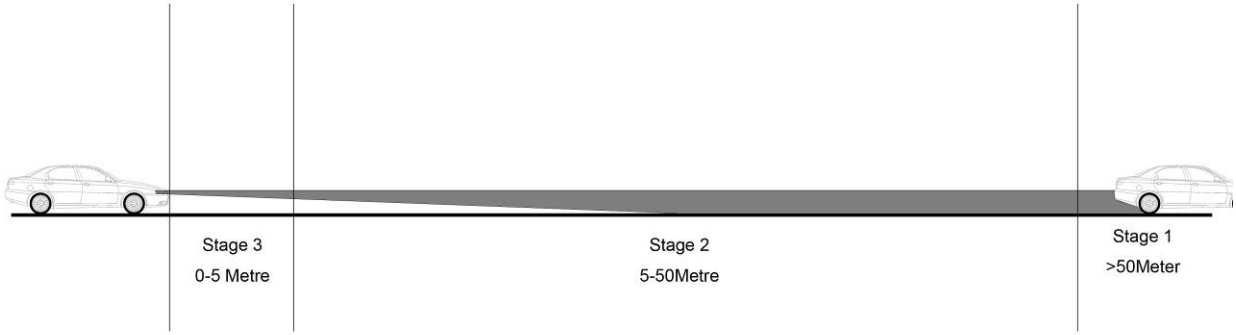

Figure 2.5: Stage 1 – Obstacle over 50 meters ahead

In Figure 2.5, the obstacle was detected at the distance of over 50 metres. High beam will be automatically switched on if there aren't any street lamps detected or highest position Low Beam will be maintained.

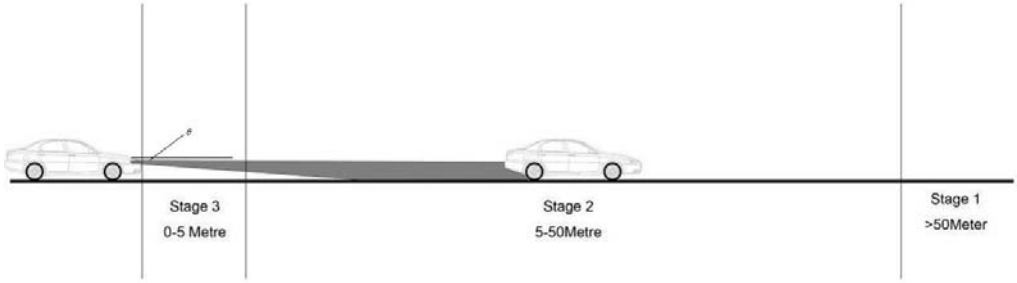

Figure 2.6: Stage 2 – Obstacle within 5-50metres

In Stage 2, the obstacle was detected in 5-50 metres area. Low beam light will be on and the angle will be adjusted automatically according to the actual distance.

The voltage output by the Ultrasonic Sensor ***v*** is inversely proportional to the distance l_1.

$$l_1 = k_{uL} \frac{1}{v} \tag{2.1}$$

where k_{uL}: is a coefficient of the ultrasonic sensor. The beam angle of headlamp θ is described by the tangent.

$$\frac{h}{l_1} = \tan\theta \tag{2.2}$$

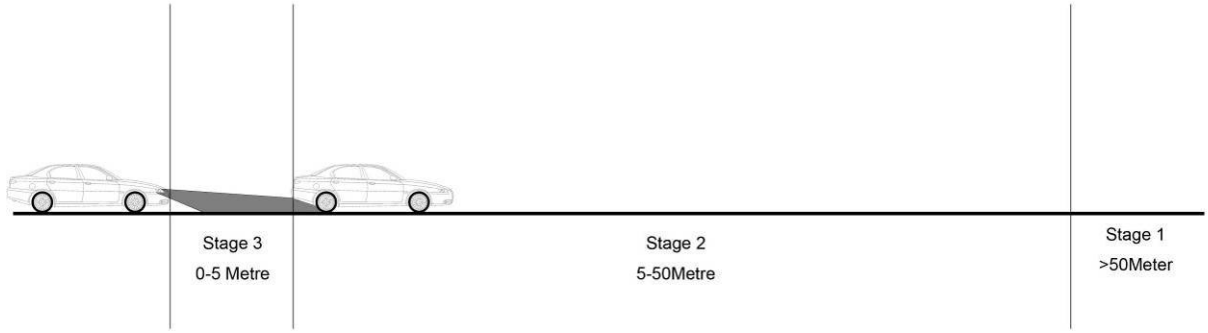

Figure 2.7: Stage 3 – Obstacles with 5 meters.

Angle of head lights is adjusted according to distance in the above cases.

2.2 Load sensor

Load Sensor on Front and Rear Suspension is shown in Fig 2.8. Parts A and B are explained as follows.

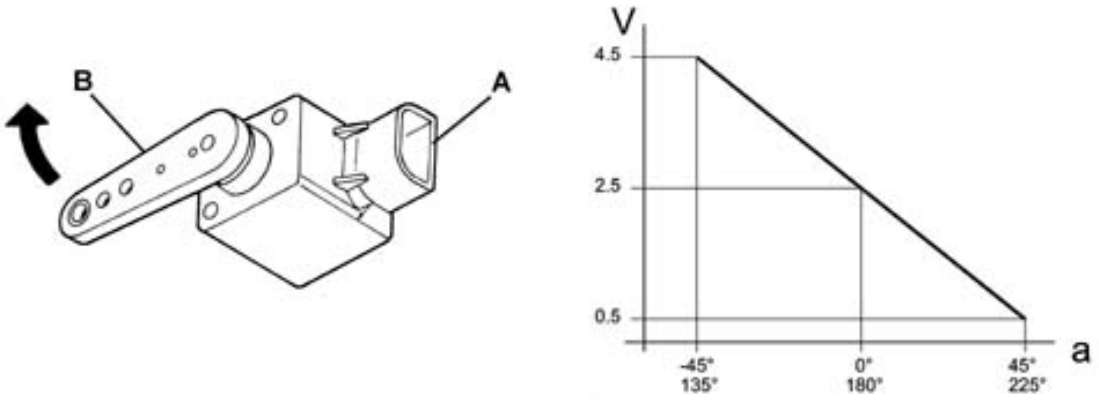

Figure 2.8 – Load Sensor and its output signal.

A – The connector to the headlamp control unit.

B – The arm of the load sensor connecting to the suspension arm that will move according to the suspension movement.

The output of the load sensor is from 0.5 - 4.5V according to the angle of the sensor arm has turned. Basically the load sensor is a kind of Hall Effect Sensor which requires 5V input.

2.3 Light Dimming

HID Dimming Control Circuit is built-in with electronic ballast. There are two methods control to dimming function, Analogue and Digital Control. Dimming control of high power metal halide lamps have been discussed in [18]-[22]. In paper [18] the dimming operation and the influence of the topology on dimming performance is discussed. The dimming operation at low frequency is implemented in [19] and [20]. The dimming control based on voltage control and frequency control is discussed in [21] and [22]. However, the above papers on dimming control are not referred to automotive application. Paper [23] introduces dimming control methods for automotive application using analogue methods. It is shown that by controlling the current gain of the controller it is possible to operate the lamp from its rated 35 W of output power to 24 W.

Light sensors on the dashboard will detect the light reflected by other obstacles in the front of the vehicle. If the level of brightness is too high which may glare the driver inside the vehicle, the HID lamp will decrease the brightness until it becomes a comfortable level. Since the dimming level of the HID lamp is limited, the Headlamp will be automatically switched off if the level of dimming cannot be met.

2.4 Automatic High/Low Beam System

The use of high-beam on roads with poor visibility may help the driver but certainly causes glare to the oncoming vehicles. Courteous driving calls for switching to low-beam to avoid glare to the opposite vehicles. Hence, any system that can automatically switch from high-beam to low-beam upon sighting the oncoming vehicle or sensing the surrounding light would be very helpful for the driver.

Automatic High/Low beam system is a system which can switch between high and low beam automatically in response to the detection of light from the oncoming traffic or surrounding light. A block diagram of this system is shown in Figure 2.9. In this system light sensors on the car upon sensing light either from the oncoming vehicle or surrounding light generate a signal to initiate switching over to low-beam driving. It will revert back to high-beam after fixed no light detection period.

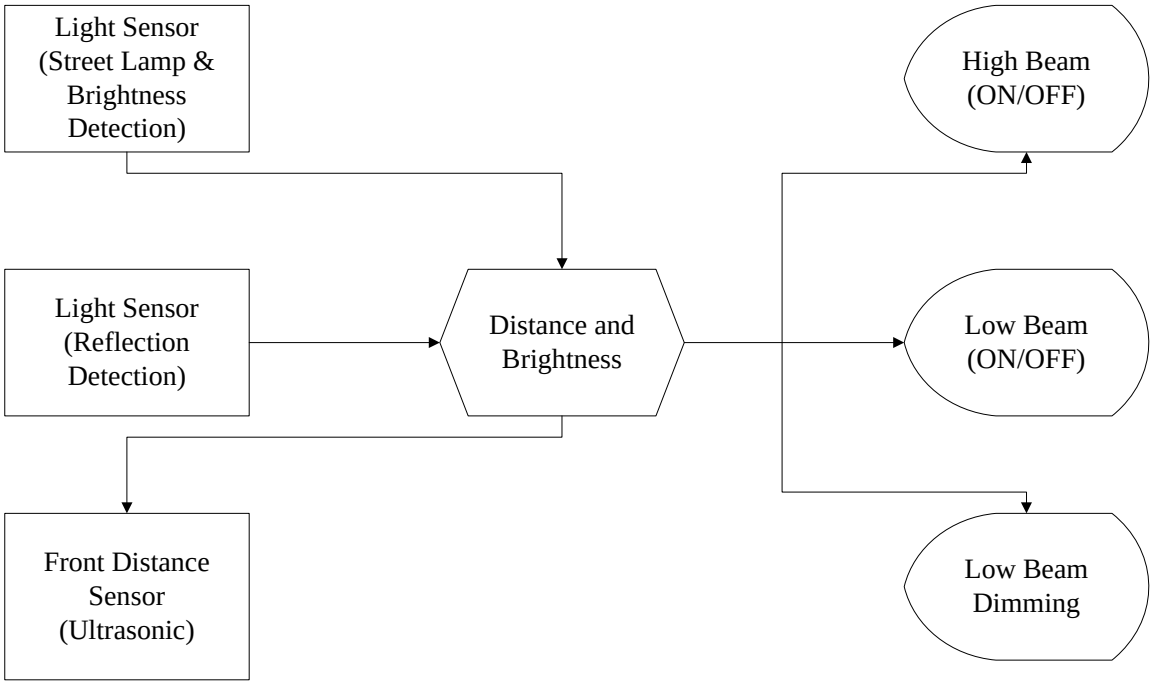

Figure 2.9: Automatic Hi/Lo Beam System with speed control

2.5 Low Beam Level Adjustment

In the present study a method is suggested to improve the performance of the level adjustment scheme discussed previously. In this new system an additional input from a sensor that detects the distance of the oncoming vehicle is used along with the inputs from the vehicle pitch detection sensor and the speed sensor. The distance detection sensor is used mainly to ensure that the projected light does not cause glare to the oncoming drivers and also to enable the low beam to project slightly over a longer distance when there is no oncoming traffic. A block diagram of the control is shown in Figure 2.10.

The motor used for the level control is a dual coil electric motor. Figure 2.11

shows a schematic diagram of an H-bridge converter for driving a 2-phase stepper motor. The H-bridge converter facilitates 4-quardant control. The output of the H-bridge converter drives each winding of the motor.

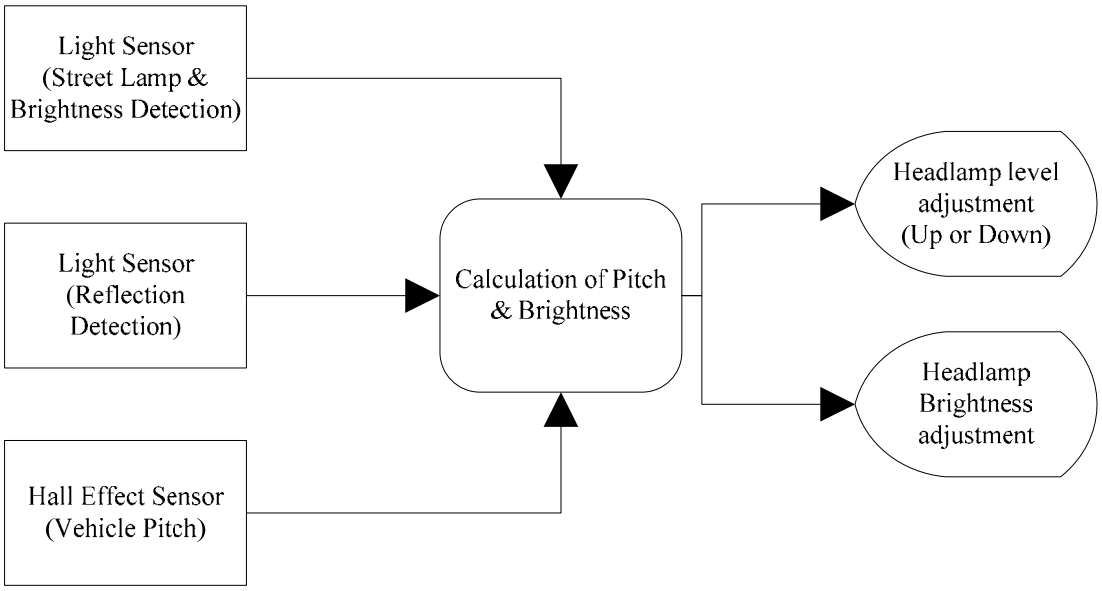

Figure 2.10: Low Beam Levelling and Dimming System

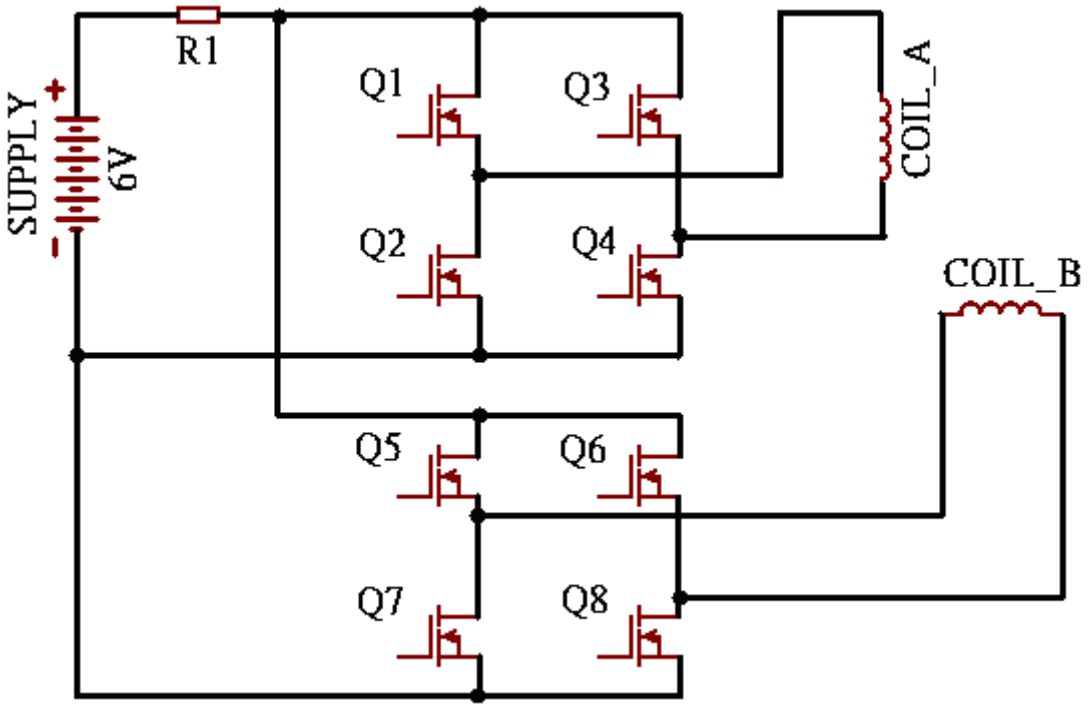

Figure 2.11: H-Bridge for Stepper Motor

Figure 2.12 shows the power supply to the H-bridge converter. For conventional design, a linear regulator is used that reduces the 12 car battery voltage to 6V. However, the efficiency is a concern as the efficiency is at most 50% because half of the voltage is reduced. For high performance AFS, the power supply should be changed to more advanced version. The detail will be presented in Chapter 4.

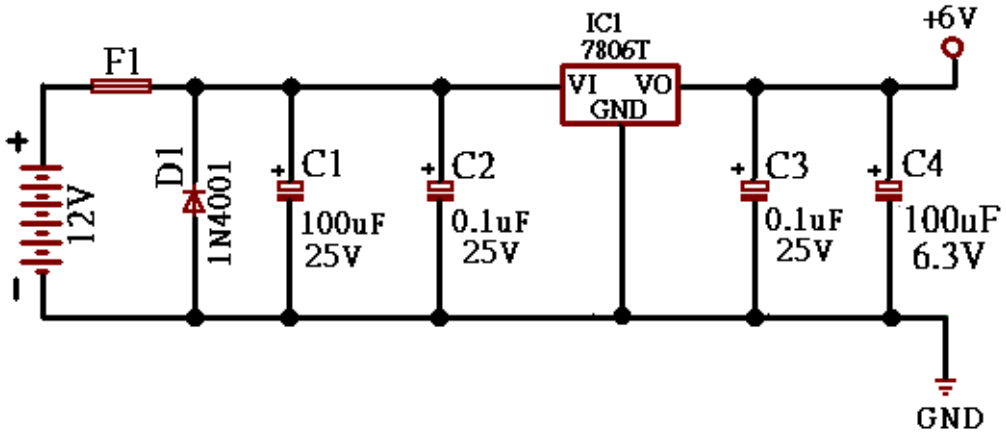

Figure 2.12: 6V Supply for Headlamp Level Control

2.6 Fail-safe

Since the design of this new system is proved to be reliable, precaution of system failure is still being considered. All the components are continuously monitored by the control unit. Signal is sent to the control unit without interrupting.

Once there are any errors detected that will lead to an override of the whole system. The deactivation of the system will maintain the headlamp level in a lowest position with maximum brightness which is the same as a lowest headlamp without active levelling system. This prevents glaring effect to the upcoming traffic and maintaining the visibility to the driver. A warning lamp will illuminate on the dashboard as a reminder to the driver sending the car to the authorized dealer for further diagnosis. Moreover, an error code will be stored inside the controller of this system as well as a warning lamp.

2.7 Vehicle Speed

The Speed of the vehicle is also one of the key factors of controlling the headlamp. The faster the vehicle travels, the longer distance the drivers should see. The headlamp should project more far away when the vehicle is travelling in the highway rather than in the city. The detection of speed can help the system to differentiate the headlamp appropriate projection area without affecting other road users.

2.8 Summary

The general operation of advanced headlamp system has been discussed in this chapter. The most important goal for designing this system is providing maximum

visibility to drivers in any conditions and preventing glare affecting other road users. To fulfil this requirement, High/Low beam control, dimming, beam level adjustment, power source as well as fail-safe system have been discussed. The sensors used in the beam control for checking the light sources and distances are also illustrated. The level adjustment is an H-bridge controller which is a simple and compact design that can control the stepper motor effectively.

Chapter 3.Simulation of Auto-levelling control system

3.1 Introduction

To verify the functionality of this system, rather than creating a real life experiment, a simulation by the software “Simulink” has been done. Through this software, a standard set of data can be created as the testing environment to compare the differences between the theory and practical results. Four criteria has been set to be the reference of the logic control which is Distance Signal, Street Lamp Sensor signal, Front Light Reflection Sensor signal and Speed Signal. These criteria will be used to calculate the logic control of the high beam and low beam of the Automatic Headlamp System. In order to show the results in a simple and clear way, assuming the pitch of the vehicle remains horizontal and velocity of vehicle remains constant.

Case 1: Automatic High/Low Beam Control

Automatic High/Low Beam is part of the headlamp control system. The result for activating the system is related to the Distance Sensor. Assuming that a half-sinusoid source is the signal generated by the ultrasonic sensor as the distance signal. From the block diagram in Figure 3.1, $u_{x,}$ u_1 & u_2 represents Ultrasonic Sensor, High beam, and Low Beam respectively. In this system, the model was built

according to the Finite State Machine theory to stateflow block and Simulink to make complex logic relationship clearer. The stateflow chart is described in Figure 3.2. The simulation result is obtained as shown in Figure 3.3 which clearly shows the logic operation when the system receives sampled distance signal.

The waveforms shown in Figure 3.3 are the signals of High beam, Low beam and distance detector respectively. Logic “1” is equivalent to “ON” state and “0” is equivalent to “OFF” state of the light. The distance transducer converts 0-50 metres to 0-5 volt. In Figure 3.3, high beam is switched off and low beam is switched ON as well as triggering the HID Dimming Control System while the obstacles are detected in the first 5 metres. When obstacles detected in 5-50 metres, high beam will turn off. Low beam angle signal varies within the value of 0.1-1 and the angle of Low beam will be adjusted from the lowest to highest angle. High beam & Low beam will go to ON state at the same time if there are no obstacles detected in or within 50 metres.

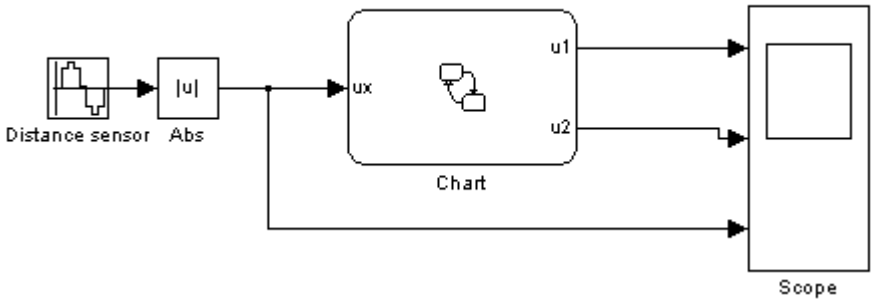

Figure 3.1: Automatic Hi/Lo Beam System

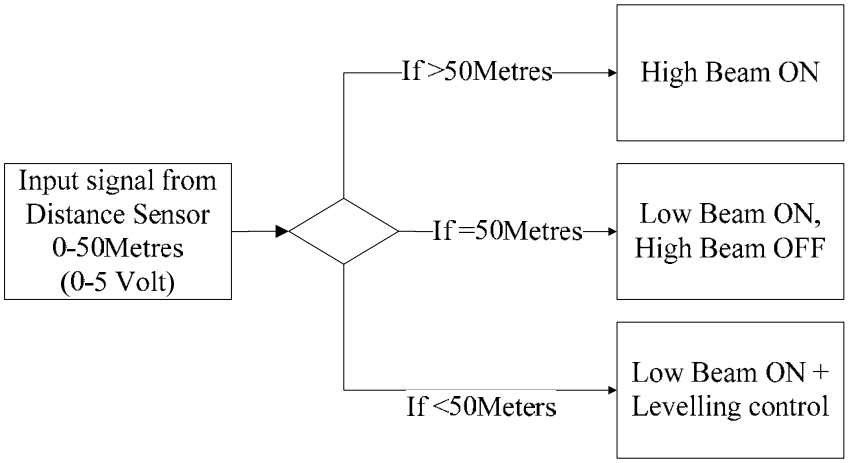

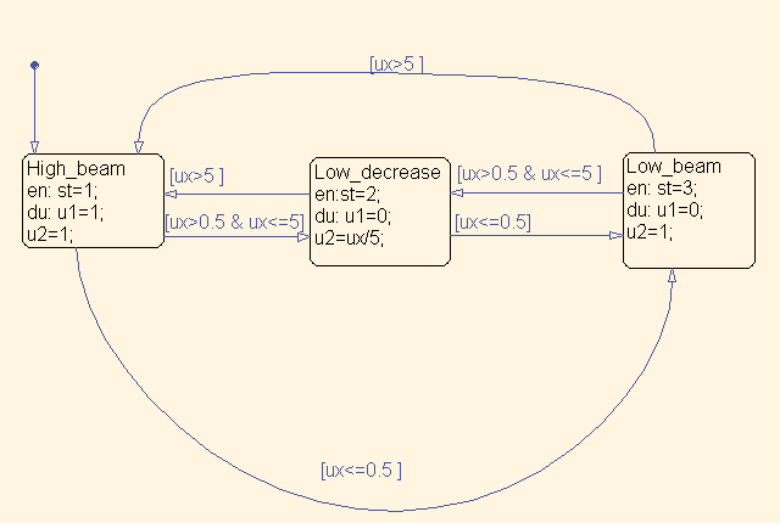

Figure 3.2: Stateflow of Automatic Hi/Lo Beam System

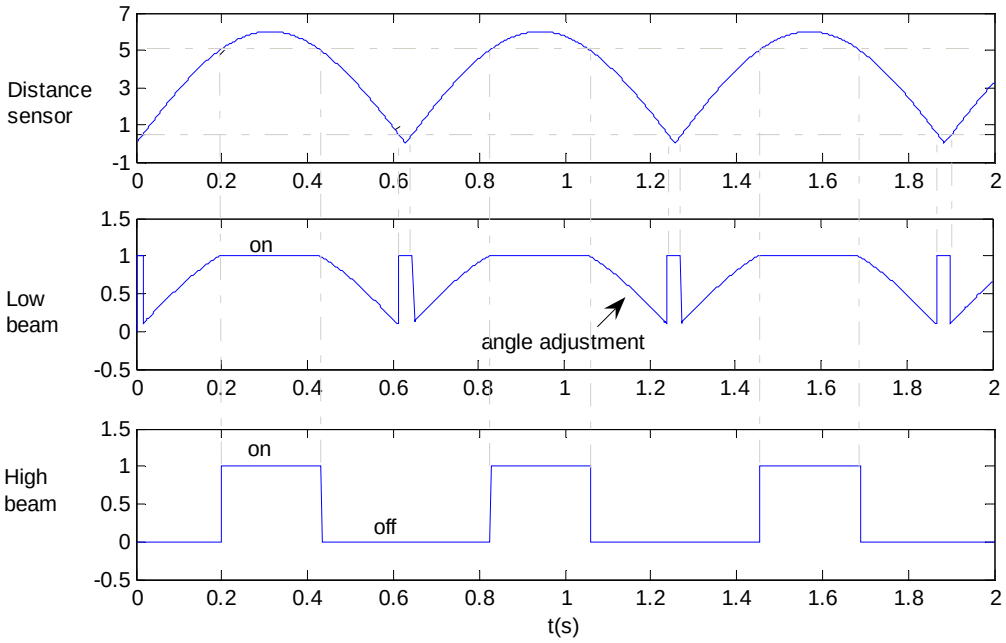

Figure 3.3: Waveforms of Hi/Lo Beam System

(Distance sensor scale: x10m)

Case 2: Simulations with Distance & Street lamp detector

A revised headlamp controlling system as shown in Figure 3.4 can vary headlamp level and High/Low beam mode according to the distance and the light upward signal which is the Street Lamp detector. A half-sinusoidal source simulates the distance signal which is sampled by the ultrasonic sensor. A pulse trains simulates Street lamp input sampled by the light upward sensor. In this system, the stateflow chart is describing the picture of the logic in Figure 3.5 and the simulation result is shown in Figure 3.6.

Light upward signal is '1' indicates a street lamp is at ON state. As the graph shown in Figure 3.6, when street lamp is detected by the street lamp sensor, the signal state is "ON", The high beam is definitely off as the street lamp is present. When street light is in "OFF" state, High beam and Low beam will be working separately according to the distance signal.

According to the designed logic, at the first cycle, street lamp has been detected by the sensor. High beam will be kept at off state since it is not necessary to use High Beam in a well illuminated road. The HID dimming control system will be triggered if the obstacle detected is within 5 meters away. The low beam is at "ON" state as well. If an obstacle is over 5 meters, the low beam angle adjustment mode will be on, and the headlamp angle will be adjusted by the distance

from 5 to 50 meters according to the actual distance.

When there are no obstacles detected within 50 metre as well as no street lamp illumination on the road, high beam and low beam will be at ON state simultaneously. High beam will be at “OFF” state again when the next street lamp is detected. Headlamp angle will be adjusted when the distance from an obstacle is less than 50 meters. The status repeats in another cycle. As it can be seen in Figure 3.1 and Figure 3.4, the only difference on two tests is to use the Street Lamp Detector signal to actuate the high beam.

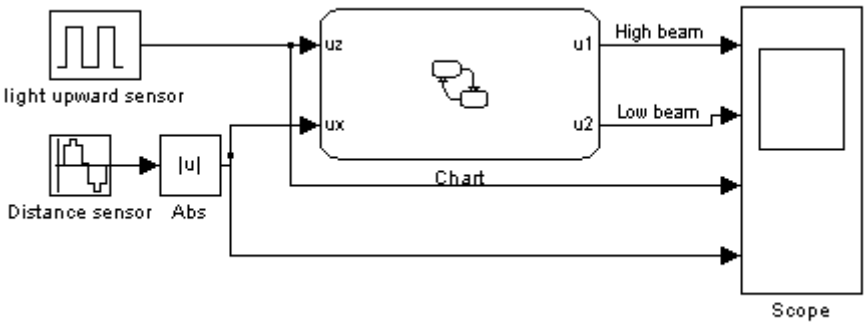

Figure 3.4: Low Beam level adjustment System

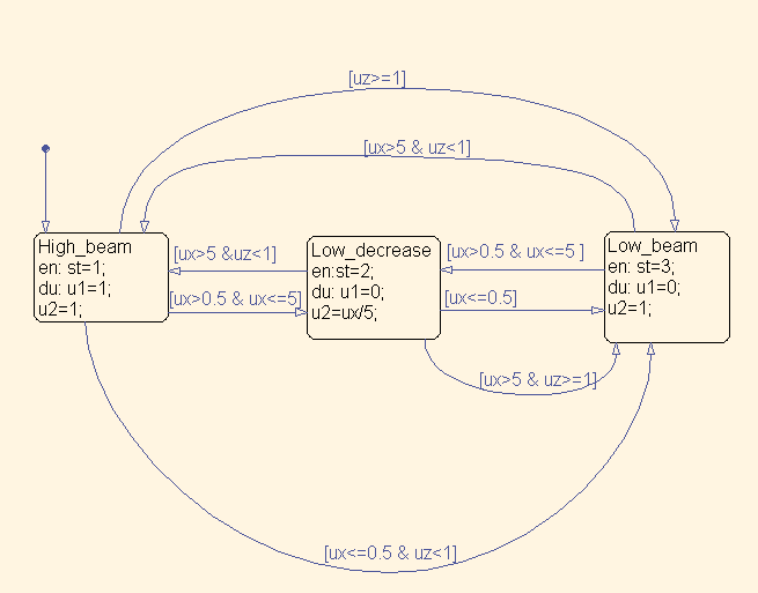

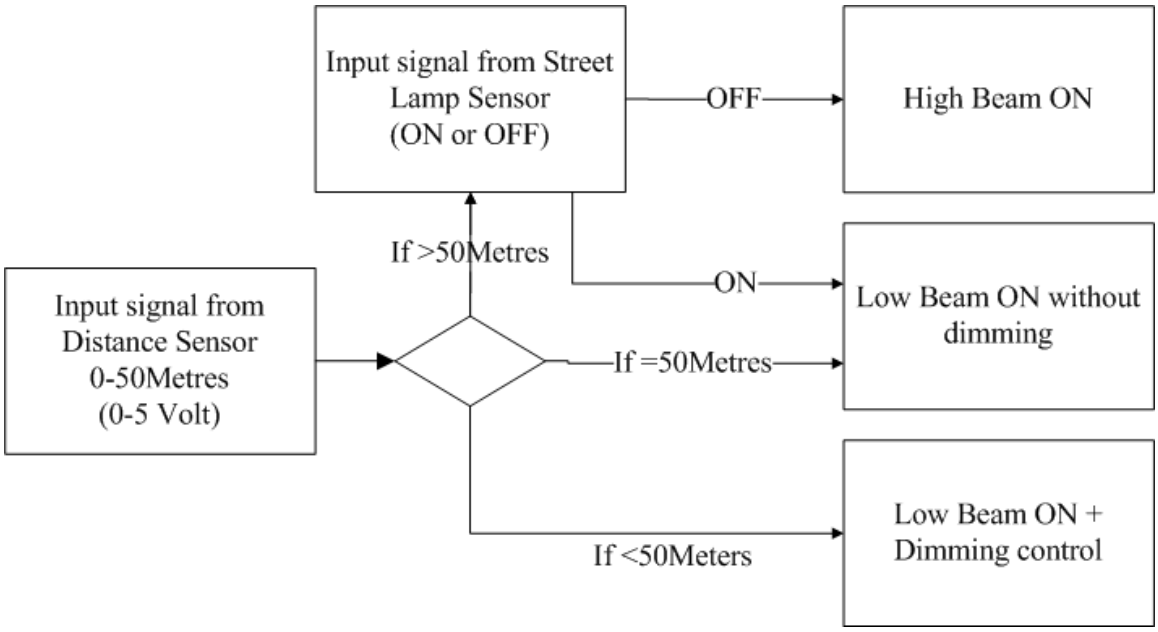

Figure 3.5. Stateflow of Low Beam level adjustment System

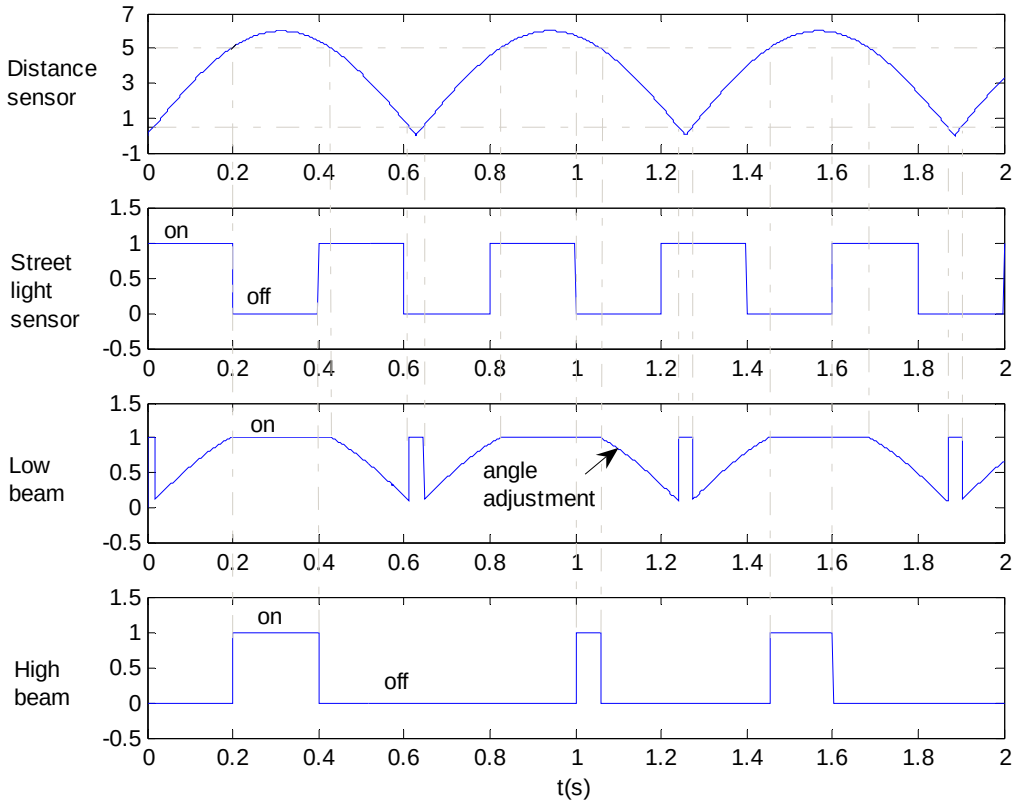

Figure 3.6 Waveforms of Low Beam level adjustment System

(Distance sensor scale: x10m)

Case 3: Simulation with Front Reflection Sensor added

Assuming a light forward sensor has been installed at the dashboard facing towards the front near the level of driver's eye-sight inside the vehicle. The function for that is detecting the headlamp beams reflected by the vehicles at the front causing glare to the driver. In this new headlamp system, dimming control system is one of the major components which collects the light from the light forward sensor and sampled into light signal. It is shown in Figure 3.7. The stateflow chart is described and the corresponding simulation result is shown in Figure 3.8 and

Figure 3.9 respectively. The high beam omitted in this case as the testing distance is not over 5 metres and the high beam is designed to be turned off. The typical distance of the obstacle is in 5 metres in our study. As shown in Figure 3.9, if the minimum brightness is over the designed brightness which the drivers can feel comfortably, low beam will be turned off completely until there are any increments in distance.

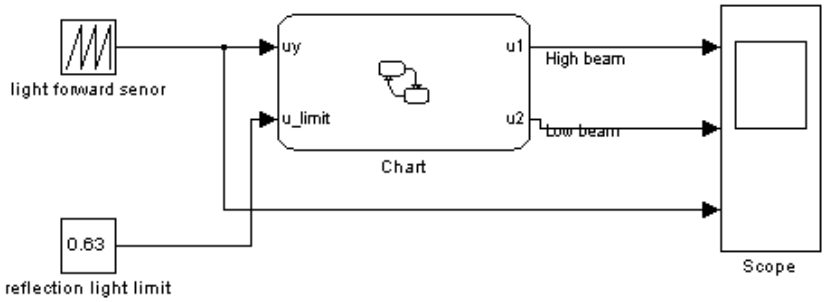

Figure 3.7 Headlamp Dimming Control System

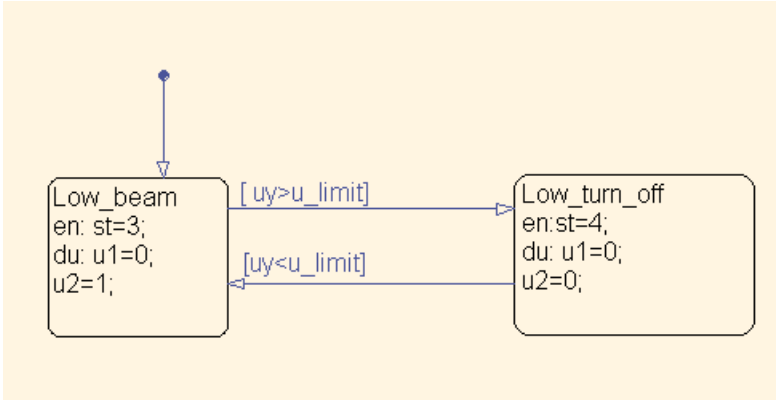

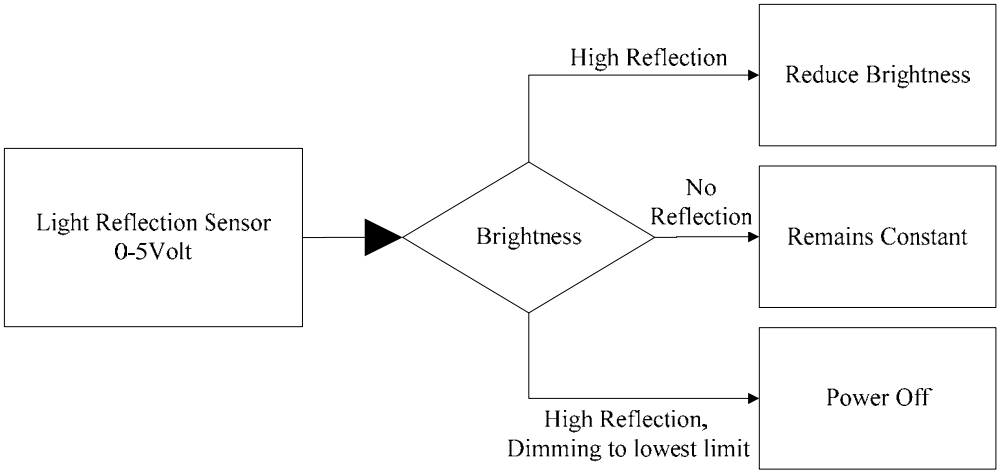

Figure 3.8 Stateflow of Headlamp Dimming Control System

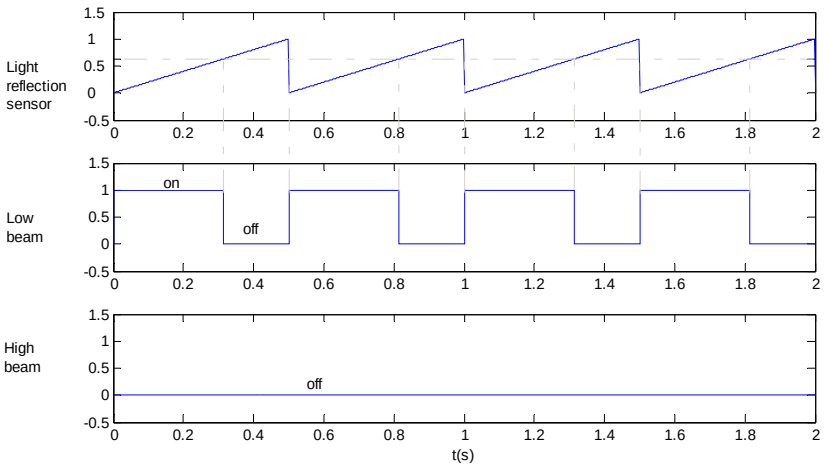

Figure 3.9: Waveforms of Headlamp Dimming Control System

(Distance sensor scale: x10m)

Case 4: Simulations with all conditions

Gathering all the simulated conditions mentioned above, a full headlamp controlling system consists of adjustable headlamp level, High beam/Low beam mode is shown in Figure 3.10. In Figure 3.11, the stateflow chart has been described and the simulation results are shown in Figure 3.12.

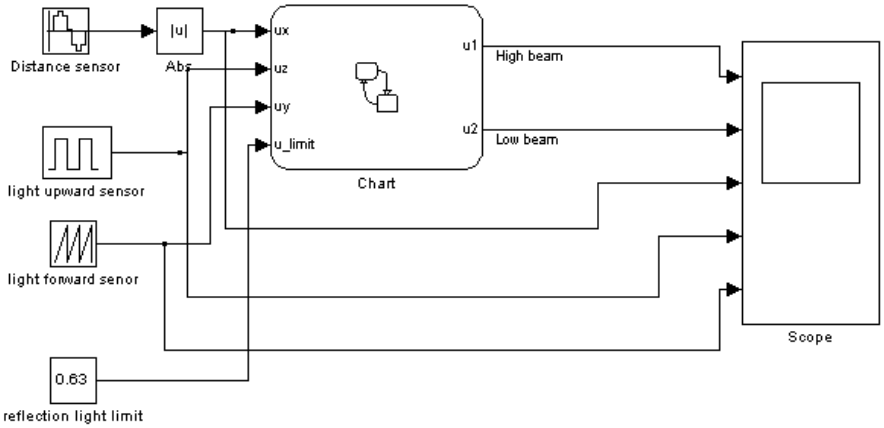

Figure 3.10: Headlamp Control System

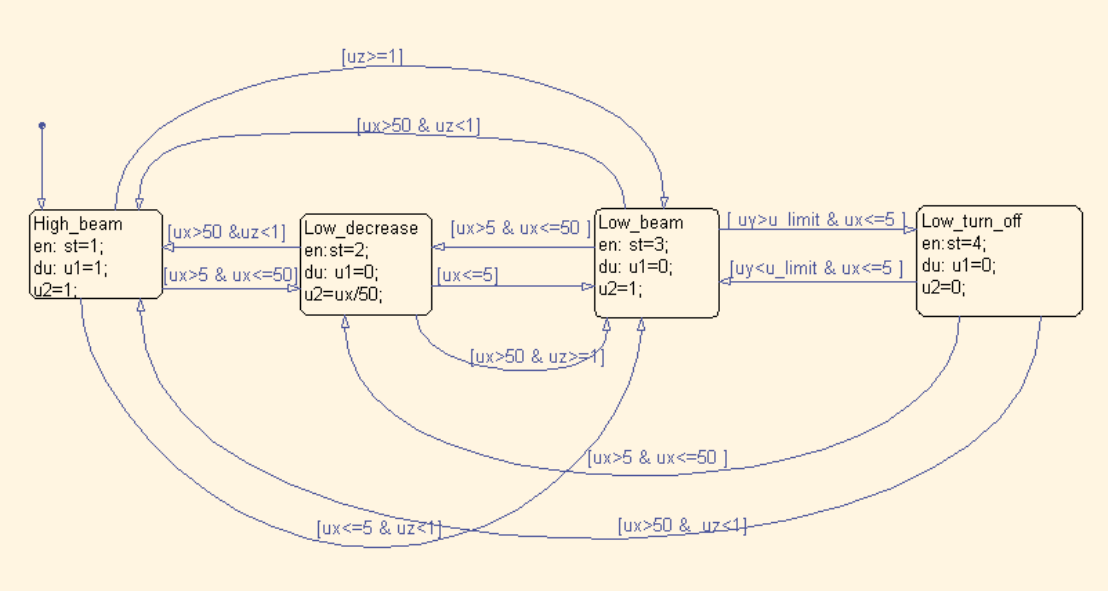

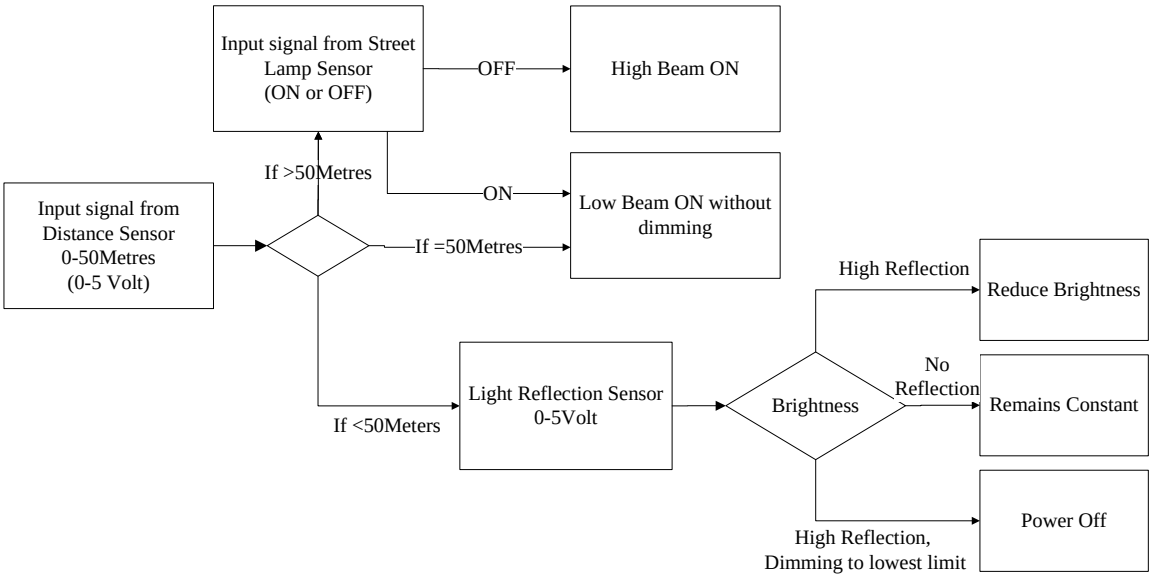

Figure 3.11: Stateflow of Headlamp Control System

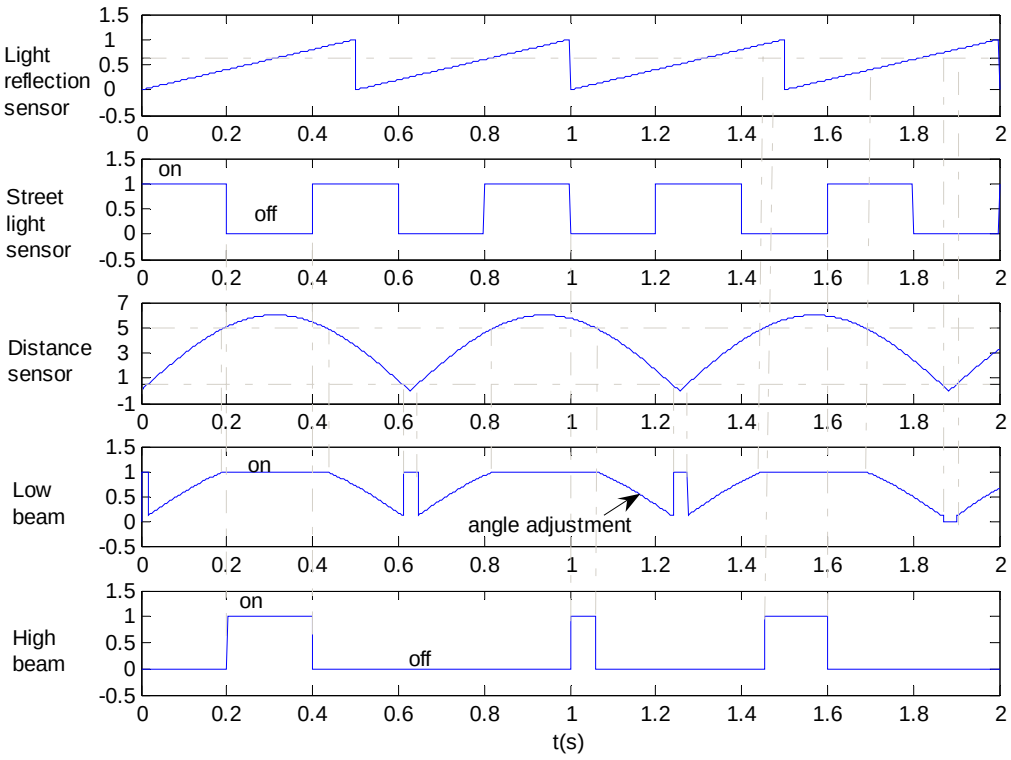

Figure 3.12: Waveforms of Headlamp Control System

(Distance sensor scale: x10m)

As shown in Figure 3.12, high beam is off in the first cycle of Street lamp sensor. If an obstacle appears in 5 meters at the same cycle and the brightness is still acceptable, the low beam is on with dimming by the HID dimming control system.

If an obstacle appears at a distance from 5 to 50 meters, then headlamp angle for Low Beam is adjusted according to the distance and High Beam is complete OFF.

In the next cycle with the street lamp detector is in OFF state, then high beam

is on because there are no obstacles detected within 50 metres. However, the high beam will be off again when an obstacle appears in 50 meters. This operation is repeating until the end of the second cycle. If the distance is in 5 meters and the brightness is over limit, low beam is also off.

3.2 Summary

The Simulink model has been presented to examine the logic flow of different parts of the Advanced Headlamp Control System. This simulation gives a clear mind on testing the functionality of our design ideas before building a physical model. The method shows developing a new system by using simulation can reduce time and failure rate. Simulation results of 4 different cases have been provided.

Chapter 4.System and power supply

4.1 The System

The system consists of the electronic ballast, HID lamp, motor drive and servo motor. The whole system is supplied from the vehicle battery 12V. Its supply voltages of the motor and drive are both 6V. Its power rating is the motor drive is as follows:

Table 4.1:The electrical specification of the motor

Loading	Power	Current
Light load	1.5W	0.25A
Full load	2.5W	0.5A

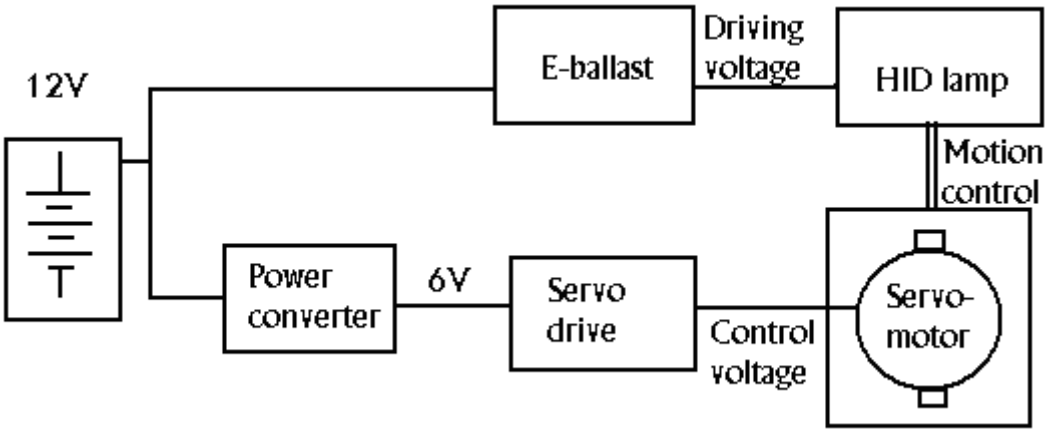

Figure 4.1: System diagram with step down converter

4.2 Power Resonant Supply

The proposed system aims to be used in a commercial vehicle at low cost. Therefore a simple power supply is proposed to reduce the 12V to 6V for the motor. One of the needs for the power supply is low electromagnetic interference (EMI) loss. The conventional switched-mode power supply such as the Buck, Cuk and Buck-boost converters may not be suitable as they are hard-switching. The EMI emission may be large to affect the performance. Therefore it is proposed to use a resonant converter.

There are many suitable candidates such as the quasi-resonant converter [24], extended period quasi-resonant converter [25], load-resonant converter [26] and phase-shifted resonant converter [27]. For the present power rating, a low power topology is more suitable. Switched-capacitor resonant converter is a simple converter that is easy to be designed and also has low EMI [28]. Old type of linear power supply may be used, but they are not good at performance in terms of efficiency.

Conventional switched-capacitor resonant converter requires two transistors. Its transistors are driven is in 50% duty ratio and in alternative excitation. The both devices are not in the common ground; therefore it requires a level-shifted gate

drive. Figure 4.2 shows the typical circuit for double mode and the half mode converters. It can be seen that the Q_1 of double mode and both transistors of half mode are required special gate drive to accommodate the level-shift problem. This makes the simple converter become complicated in design.

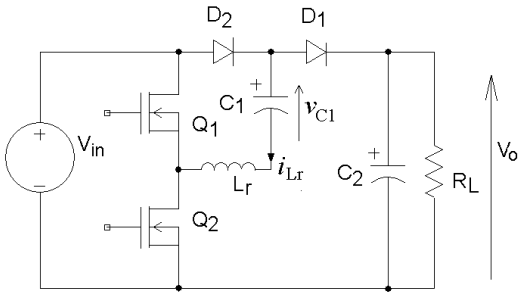

(a) double mode

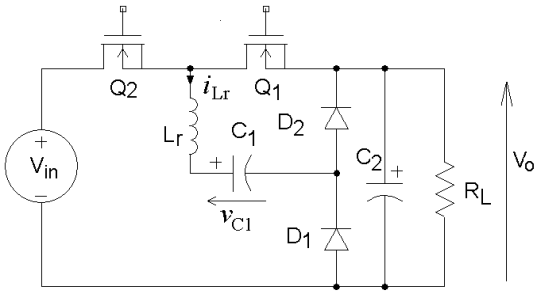

(b) half mode

Figure 4.2: Switched-capacitor resonant converters

Switched-capacitor converters have been discussed extensively in the research areas domain. This includes the multiple output [29], step-down converter [30], step-up converter [31] and power factor correction [32]. This chapter is to examine

the alternative method to implement a simple switched-capacitor resonant converter.

4.3 New Gate Drive Arrangement

The converter needed for the present application is a step-down converter that reduces the 12V car battery to 6V for the servo-drive. Therefore a half mode switched capacitor resonant converter is suitable. The converter can easily reduce the voltage by half without complicated controller. However, the gate drive arrangement must be simplified.

Usually this converter is driven by optical gate-drive, isolated pulse transformer or level-shifted gate-drive. The present solution as shown in Figure 4.3 is to use a 50% oscillator to drive the transistor and also an N-channel and a P-channel MOSFET are used for the Q_1 and Q_2 transistors.

Fig 4.3 shows the proposed circuit of the new gate drive. In the circuit, V_{G1} and V_{DS1} are the gate-source and Drain –source voltages of the Mosfet Q_1. V_{G2} and V_{DS2} are the gate-source and Drain –source voltages of the Mosfet Q_2.

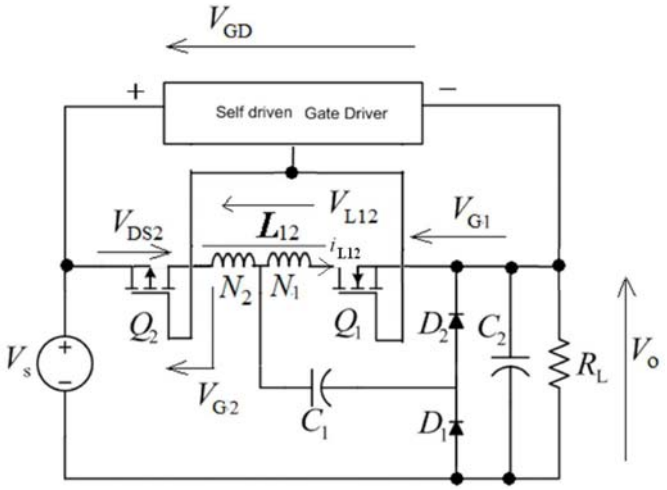

Figure 4.3: Proposed simplified driving method for switched-capacitor resonant converter

The oscillation frequency of this oscillator is fixed by the value of capacitor (C) and resistor (Ra) and resistor (Rb).

Roughly oscillation frequency can be calculated by the following formula.

Because there is an error of the part, the oscillation frequency of the actual circuit is sometimes different from the calculated value little.

$$f = \frac{1.44}{(Ra + 2Rb) \times C}$$

Unit f : Hz / C : Farad / Ra and Rb : ohm

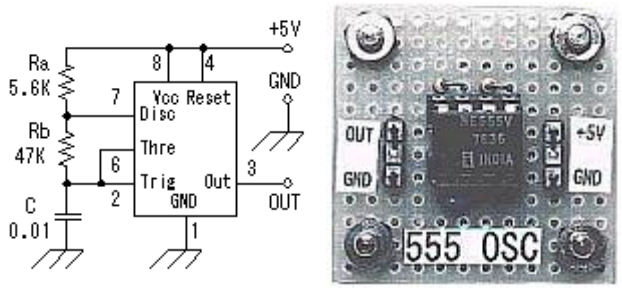

Fig 4.3a the cheapest oscillator, The IC is called 555.

Calculate the frequency for your circuit and obtain Ra and Rb and C; Usually Ra and Rb are using k Ohm, C are uF.

Change the voltage to Vin=6V from +5V form the circuit.

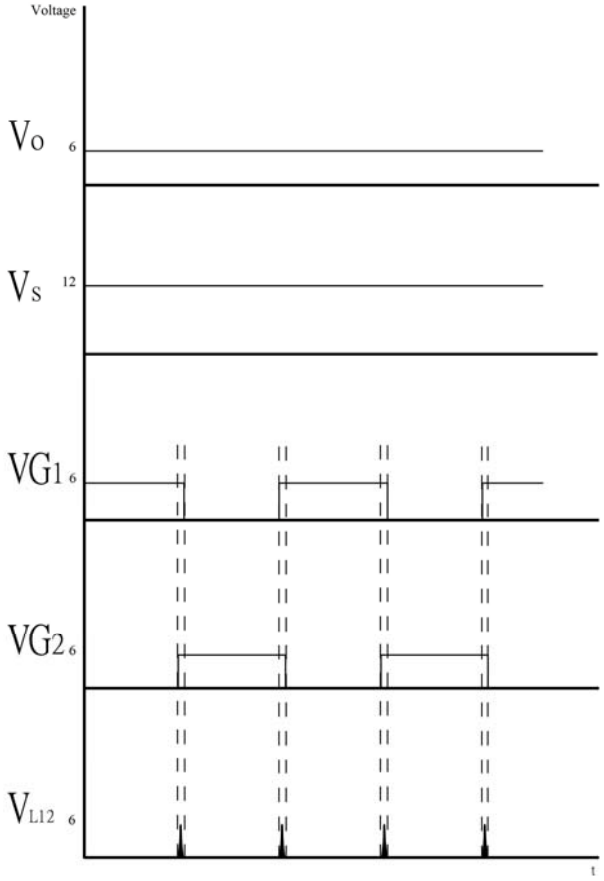

Figure 4.3b: Waveform of V_o, V_s, VG_1, VG_2 & V_{L12}

L_{12} is a small inductor that stops any short circuit between the two transistors during switching instant. N_2 and N_1 are the number of turns of the tapped inductor near Q_2 and Q_1 respectively.

Using P and N channels for push-push gate drive is a common method for driving half-drive circuit. Bipolar transistor such as PNP and NPN can also be

used. The self-driven gate drive is a simple 50% duty oscillator. In steady-state, the supply voltage to the self-driven gate drive V_{GD} is given by:

$$V_{GD} = V_S - V_o \tag{4.1}$$

In steady-state, V_o is 6V, V_{GD} is 6V. This is suitable for the self-driven gate drive. During transient, V_o will increase from 0V to 6V, V_{GD} will drop from 12V to 6V. This is also suitable for the proposed self-driven gate drive as the simple oscillator can usually work under a wide range of voltage.

4.4 Deadtime

The usual practice is to implement the deadtime in the gate drive for Q2 and Q1 in order to eliminate the shoot-through short-circuit. For the simple circuit being discussed, an inductor L12 is added to ensure there is no high current. The overlapping time is usually very short and in the range of several to 200 of ns. After the overlapping, the voltage across L12, VL12, become part of the resonance voltage with C1. The Gate drive voltage for the two transistors Q2 and Q1 are governed by VQ2 and VQ1 respectively:

$$V_{GD} = V_{G1} - V_{G2} \tag{4.2}$$

The square waveform generated by the self-driven gate drive is V_{G1}. V_{L12} is non-zero during the overlapping period and it becomes resonance voltage afterwards. In general, when V_{G1} is excited to 6V, Q_1 is turned on, and V_{G2} is 0V. When V_{G1} is off or becomes 0V, V_{G2} is -6V and Q_2.is turned on.

4.5 Resonant Circuit Formulation

Figure 4.4 shows the equivalent circuit during the different stages of operation. Figure 4.5 shows the time diagram. The description of the circuit is as follows:

State I: Overlapping ($t_0 - t_0$')

Overlapping is due to simultaneous conduction of Q_1 and Q_2. The inductor L_{12} is then impressed by V_{GD}.

Therefore:

$$L_{12}\frac{di_{L12}}{dt} = V_{GD} \qquad (4.3)$$

where L_{12} is the overlapping current and is also the current through L_{12}. Assume the overlapping time is T_{ov}, then i_{L12} will increase to:

$$v_{C1} = V_o + I_{p3} Z \cos(\pi + \omega T_{ov}) \tag{4.4}$$

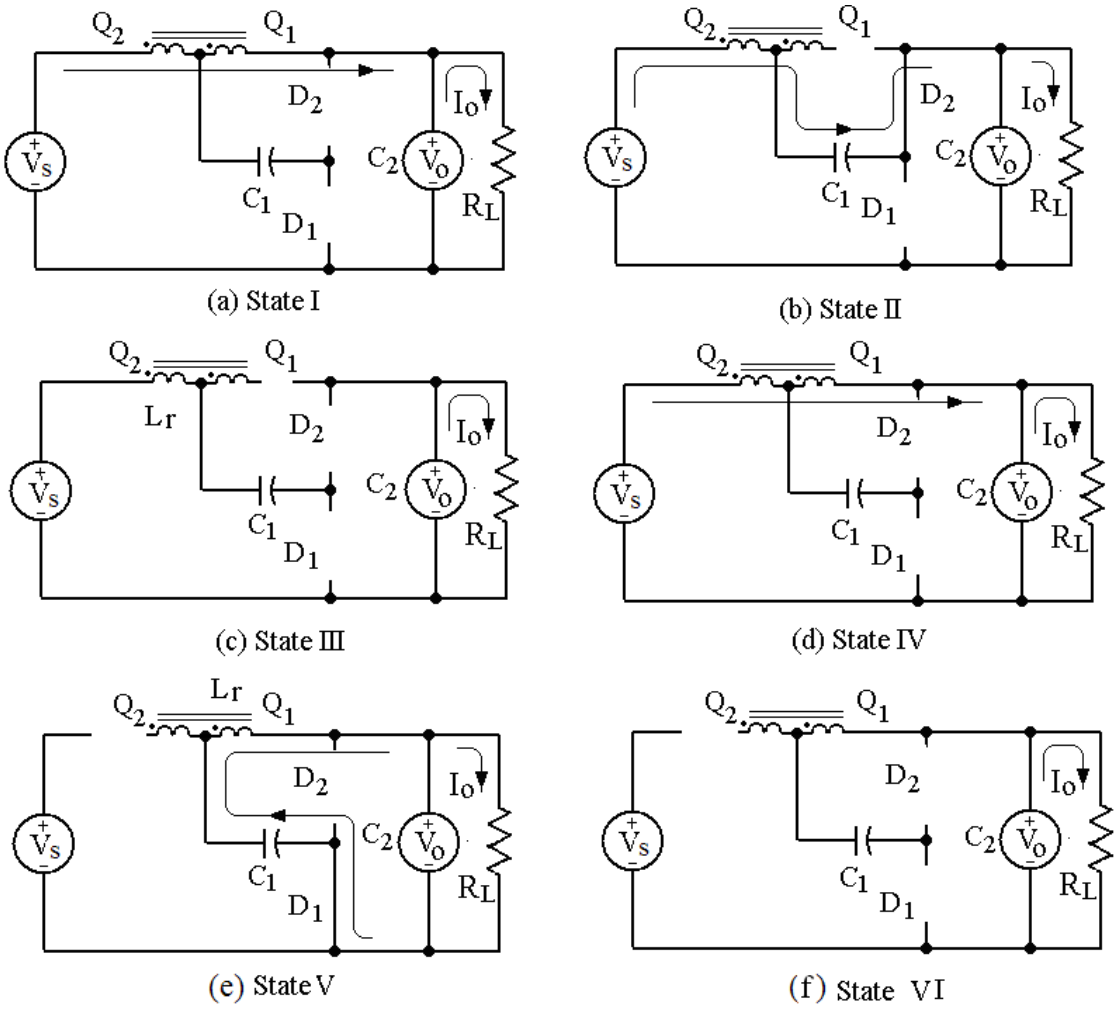

Figure 4.4 States of operations of the half mode version

Q_1 is then turned off; the energy stored in L_{12} is then transferred to inductor formed by N_2. Fig 4.6 illustrates current change in a step manner in a tapped inductor. The current is then:

$$I_{12N2} = \frac{V_{DG} T_{ov}}{L_{12}} \cdot \frac{N_{12}}{N_2} \tag{4.5}$$

State II: Resonance (t_0'-t_1)

Q_2 conducts. The resonance inductor L_r is now equal to L_2, and C_1 will resonate together. The state equations are:

$$V_{in} = L_r \frac{di_{Lr}}{dt} + v_{C1} + V_o \tag{4.6}$$

$$C_1 \frac{dv_{C1}}{dt} = i_{Lr} \tag{4.7}$$

The solutions are:

$$i_{Lr} = I_{p1} \sin \omega_o (t_o) \tag{4.8}$$

$$v_{C1} = V_{in} - V_o - I_{p1} Z \cos \omega_o (t) \tag{4.9}$$

where the resonant angular frequency of this state:

$$\omega_o = \frac{1}{\sqrt{L_r C_1}} \tag{4.10}$$

The resonant impedance of this state:

$$Z = \sqrt{\frac{L_r}{C_1}} \tag{4.11}$$

State III: Non-conducting on Q_2 (t_1-t_2)

All transistors are non-conducting. No special feature is reported. The resonant capacitor voltage is unchanged during this state.

$$v_{C1} = V_{in} - V_o - I_{p1} Z \cos(\pi + T_{ov}) \qquad (4.12)$$

State IV: Overlapping (t_2-t_2')

There is similar overlapping current through Q_1 and Q_2 during the instant of gate signal of Q_2 is being turned off and Q_1 is to be turned on. Assume the overlapping time is the same T_{ov} then i_{L12} will increase to:

$$I_{12} = \frac{V_{DG} T_{ov}}{L_{12}} \qquad (4.13)$$

Q_2 is then turned off; the energy stored in L_{12} is then transferred to inductor formed by the N_1. The current is then:

$$I_{12N1} = \frac{V_{DG} T_{ov}}{L_{12}} \cdot \frac{N_{12}}{N_1} \qquad (4.14)$$

Usually, N_1=N_2, therefore

$$I_{12N1} = \frac{2V_{DG} T_{ov}}{L_{12}} = I_{12N2} = I_{OV} \qquad (4.15)$$

State V: Resonance (t_2-t_3)

The resonance inductance L_r is now equal L_1, and C_1 start to resonate together.

The state equations are:

$$v_{C1} + L_r \frac{di_{Lr}}{dt} = V_o \tag{4.16}$$

$$i_{Lr} = C_1 \frac{dv_{C1}}{dt} \tag{4.17}$$

The solutions are:

$$v_{C1} = V_0 + ZI_{p3} \cos \omega_o t \tag{4.18}$$

$$i_{Lr} = -I_{p3} \sin \omega_o t \tag{4.19}$$

f. State V: Non-conducting on Q_1 (t_3-t_4)

This happens when the current drops to zero, the resonance ends and the main components are all off. The resonant capacitor voltage is unchanged at:

$$v_{C1} = V_o + I_{p3} Z \cos(\pi + T_{ov}) \tag{4.20}$$

4.6 Boundary Condition and Calculation of Current Amplitude

The capacitor voltage V_{Cr} at t_1 should be equal to V_{Cr} at t_2. Also C_r at t_4 should also be equal to V_{Cr} at t_3. Therefore, by equating the boundary conditions, and equating (4.9) to (4.20) and (4.12) to (4.18), it follows that:

$$I_{p1} = I_{p3} \tag{4.21}$$

The amplitude of I_{p1}can be obtained by the average input current I_{in}.

The input current only flows during States I-III, therefore the average of the i_{Lr} during the period can be used to estimate the amplitude of I_{p1}.

$$I_{in} = (I_{p1} + I_{12N2})\frac{2}{\pi}\frac{T_r/2 + 2T_{ov}}{T_s} = (I_{p1} + I_{ov})\frac{T_r + 4T_{ov}}{\pi T_s} \qquad (4.22)$$

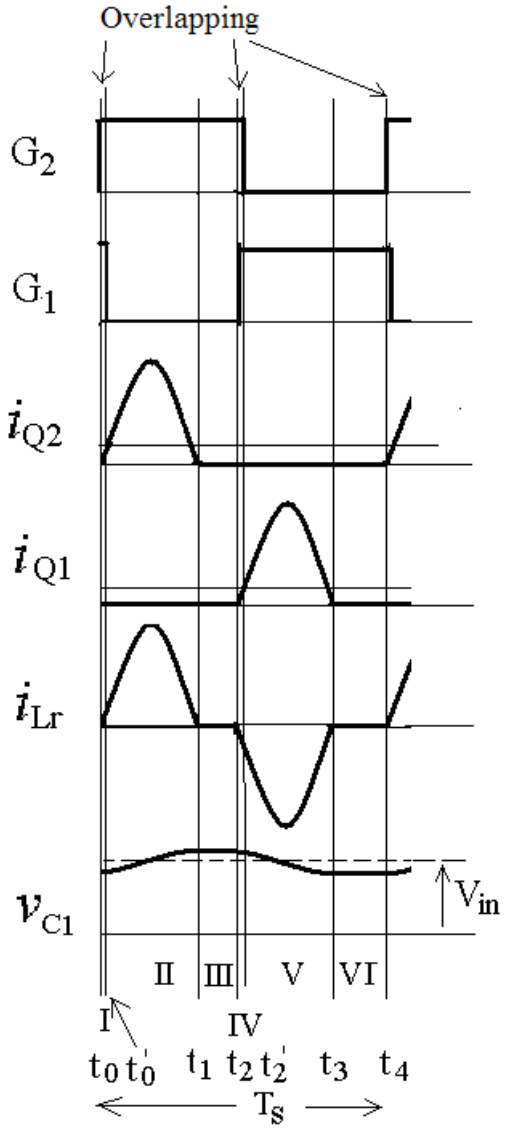

Figure 4.5 Time diagram of the converter

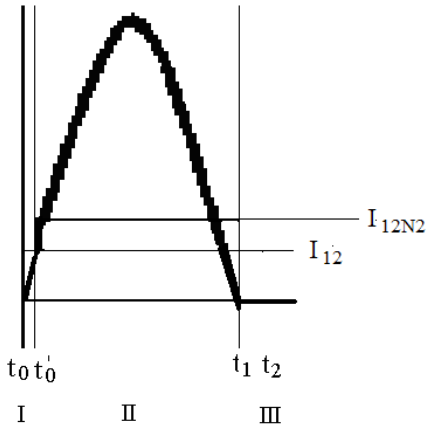

Figure 4.6: The zoom in of i_{Lr} to illustrate the overlapping in State I and step-current transition to State II.

The average output current I_o can also be used to estimate the amplitude of I_{p3} based on the conduction of Q_1 during Stages IV- VI and conduction of Q_2 during Stages I-III.

$$\begin{aligned} I_0 &= (I_{p1} + I_{12N2})\frac{2}{\pi}\frac{T_r/2 + 2T_{ov}}{T_s} + (I_{p1} + I_{12N1})\frac{2}{\pi}\frac{T_r/2 + 2T_{ov}}{T_s} \\ &= (I_{p1} + I_{ov})\frac{2T_r + 8T_{ov}}{\pi T_s} \end{aligned} \tag{4.23}$$

Eqn (4.22) and (4.23) give the relationship of input and output currents:

$$I_0 = 2I_{in} \tag{4.24}$$

Therefore the voltage conversion can be calculated by energy balance:

$$\frac{V_0}{V_{in}} = \frac{1}{2} \tag{4.25}$$

The converter still has the same feature of the original half mode voltage conversion.

The ripple voltage on C_1 can be obtained from the resonant capacitor equations (4.9) and (4.18). This gives:

$$\Delta v_{C1} = \frac{\pi I_o Z T_s}{2T_r + 8T_{ov}} \approx \frac{\pi I_o Z T_s}{2T_r} \tag{4.26}$$

4.7 Experimental Results

The above converter has been designed using the specification of:

V_s=12V

V_o=6V

Switching frequency=200kHz

Power = 2.5W

The components for both Mosfets 30V 2A and diodes 30V 2A are using low voltage type to reduce the on-state voltage drop.

For a ripple voltage of 0.1V, C_1 can be designed using Eqn (4.27). The switching resonant frequency ω_o is slightly higher than the switching frequency by 10%. The maximum voltage across the transistors and diodes are 6V. The transistor must be low threshold voltage for such low voltage application. Together with the ripple, transient voltage and tolerance of voltage stress, 30V transistors have been selected. The components used in the prototype are shown in Table 4.2.

Table 4.2 List of Components used in the prototype

Part	Parameters	Remark
Q_1	30V	P-channel
Q_2	30V	N-channel
D_1, D_2	30V	Sckottky diode
C_1	5.2μF	Polypropylene
L_r	0.1μH	Air-core

The design of the tapped inductor is based on the allowable overlapping current during the overlapping stage. As shown in Figure 4.7, I_{12} can be given by eqn (4). If $N_1=N_2$, $L_{12}=4L_1=4L_2$. L_r can be part of L_1 or L_2. When Q_2 is on and Q_1 is off, $L_1=Lr$, Similarly, When Q_1 is off and Q_1 is on, $L_2=L$. T_{ov} is the transistor overlapping time and is close to the rise or the fall time.Using $T_{ov}=5ns$, $V_{DG}=6V$, $L_{12}=4\mu H$.

$$I_{12} = \frac{V_{DG} T_{ov}}{L_{12}} = 0.075A \qquad (4.27)$$

Therefore $I_{12N1}=0.15A$. This is the rise current in stages 1 and 3. This designed value is suitable for the converter as it is only a small fraction of the resonant current.

The experimental waveforms in the steady-state are shown in Figure 4.7. It can be seen that the current of the transistor is under zero-current switching. It is also observed that the resonance current waveforms for Q_2 is slightly different from the resonant waveforms for Q_1. It is due to the two transistors are not exactly equal and its internal on-state resistance affects the practical waveforms as compared with theory.

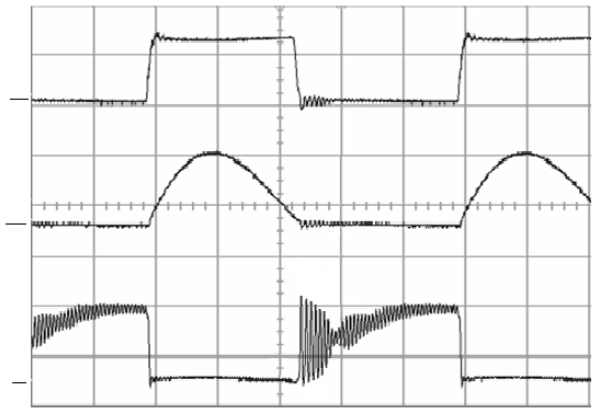

Figure 4.7: Experimental waveforms.

(Top: Gatedrive for Q_2: 5V/div; Middle: Q_2 current, 0.1A/div

Bottom: 5V/div; Time base: 1μs/div)

The efficiency of the converter has been examined. The measured results at V_{in}=12.5V of battery voltage are shown in Figure 4.8. It is clear than the efficiency is high and the voltage can be regulated within 10%.

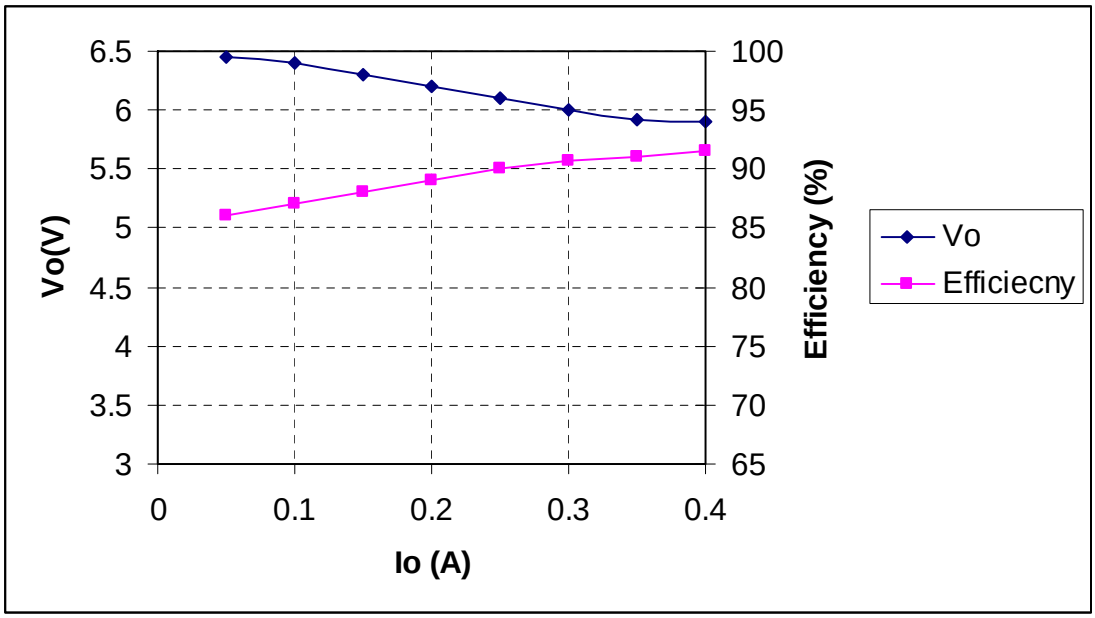

Figure 4.8 Measured output voltage and efficiency of the proposed converter

4.8 Conclusion

A simple gate-drive designed of switched-capacitor resonant converter has been proposed. The converter does not require level-shifted gate-driver. Using the p-channel and n-channel transistors, a simple oscillator can be applied to the transistor to perform the gate drive signalling. The overlapping during the two-transistor switching transient is eliminated by a centre-tapped inductor. It has been found that the high current shoot-through problem during overlapping has been eliminated. The transistor current is under zero-current switching and therefore the EMI and switching loss are small.

The converter has been used in the power supply unit of the AFS. The voltage

regulation is good and within 10%. The efficiency is high and in the 90% region. The overall performance is highly satisfactory.

The proposed converter can also be used for high power application. Typically application includes conversion of 12V to 24V for lorry applications and the conversion of 24V to 48V for electric golf cart vehicle applications. Reference [31] shows the original circuit for set-up applications, using the same deadtime control as proposed by this paper, the set-up or other voltage conversion version can be realized

Chapter 5. DC motor for headlight vertical aim control

5.1 Control formulation of the lamp using DC motor

The DC motor has been widely used in industry because it has high power density, large torque and high efficiency. In the proposed automotive headlight system, stepping motor is used because it has simple control structure and easy implementation. However, the performance of stepping motor is affected by the fixed step angle, which leads to a poor position control if one uses a low resolution motor to handle headlight position control. In this section, we will propose an alternative algorithm for headlight vertical by using DC motor. The closed-loop control scheme can improve the speed and position performance in headlight position control. Fig. 5.1 shows the proposed scheme for dc drive control. Fig 5.2 shows the model of the motor.

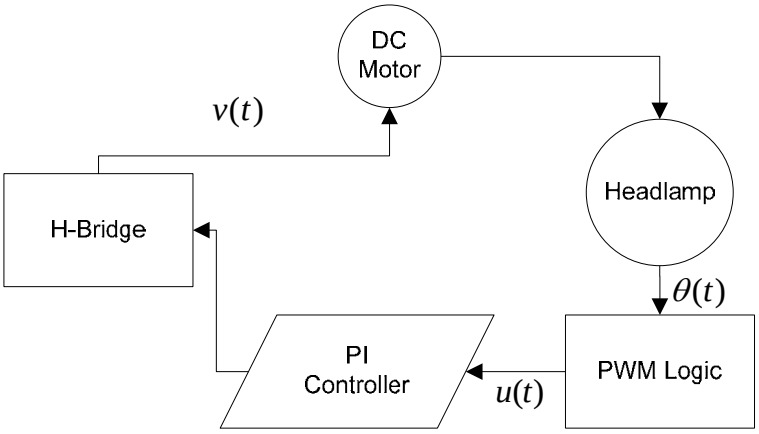

Figure 5.1 Block diagram of position control

Consider the following DC motor schematic circuit which the equivalent armature resistance R and armature inductance L are shown:

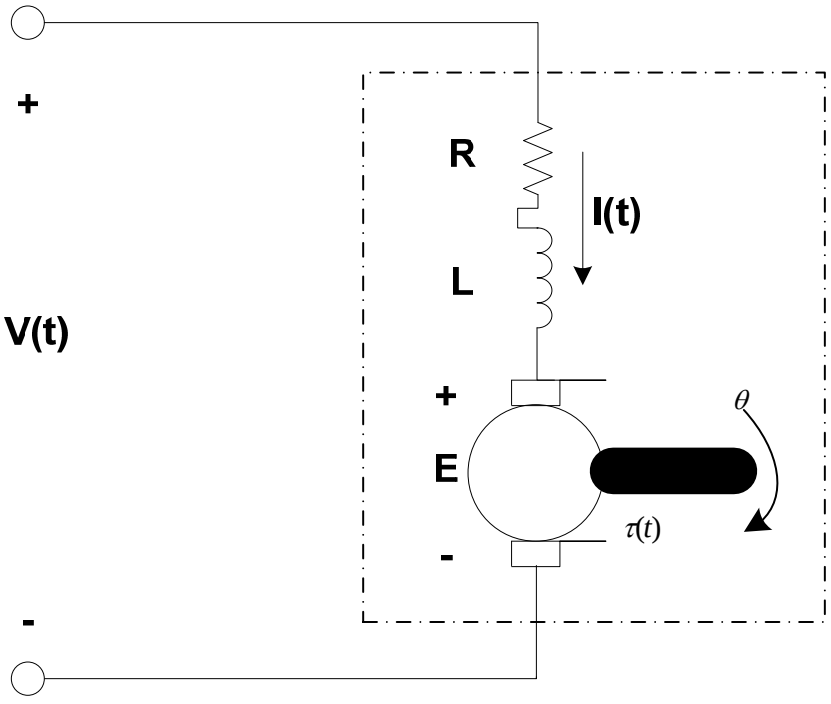

Figure 5.2 DC motor circuits in the time domain

Based on Kirchhoff's law and Newton's law, a set of differential equations can be obtained.

$$
\begin{aligned}
&Ri(t) + L\frac{di(t)}{dt} + K_e\dot{\theta} = v(t) \\
&\tau(t) = J\frac{d}{dt}\dot{\theta}(t) + D\dot{\theta}(t) \\
&\tau(t) = K_i i(t)
\end{aligned}
\qquad (5.1)
$$

where θ is the rotor position, $\dot{\theta}$ is the rotor angular speed, *i(t)* is the armature current, *τ(t)* is the motor torque, *v(t)* is the source voltage, $R=4\,\Omega$ is the resistance, $L=1.75mH$ is the inductance, $k_e=00274V{\cdot}s{\cdot}rad^{-1}$ is the emf constant, $k_i=0.0274Nm{\cdot}A^{-1}$ is the armature constant, $J=3.22\mu kg{\cdot}m^2$ is the moment of inertia and $B=3.5\mu N{\cdot}ms$ is the damping factor. Using Laplace Transforms, equation (5.1) can be expressed in s-domain.

$$
\frac{\theta(s)}{V(s)} = \frac{K_i}{s((Js+b)(Ls+R)+K_iK_e)} \qquad (5.2)
$$

5.2 The PI controller

In the headlight position control, the control task is to force the actual position *θ(t)* to follow a desired reference position $\theta^*(t)$ with small overshoot, fast settling time and no steady-state error. A PI controller is used for the headlight position control system due to its simple structure and easy implementation. The output of the PI controller is in the form of

$$u(t) = K_p e(t) + \frac{1}{T_i}\int e(t)dt$$

$$e(t) = \theta^*(t) - \theta(t) \qquad (5.3)$$

where K_p , T_i and $u(t)$ are the proportional gain, integral time constant and controller output, respectively. The parameters of the PI controller used for simulation are $K_p=1.8$ and $T_i=20$. Figure 5.3 shows the open-loop response for the DC motor system and it cannot cope with position control. However, it is seen in Figure 5.4, the closed-loop method can successfully track the set-point. The loop response has been calibration by trial and error of the K_p and T_i in order to obtain the best response.

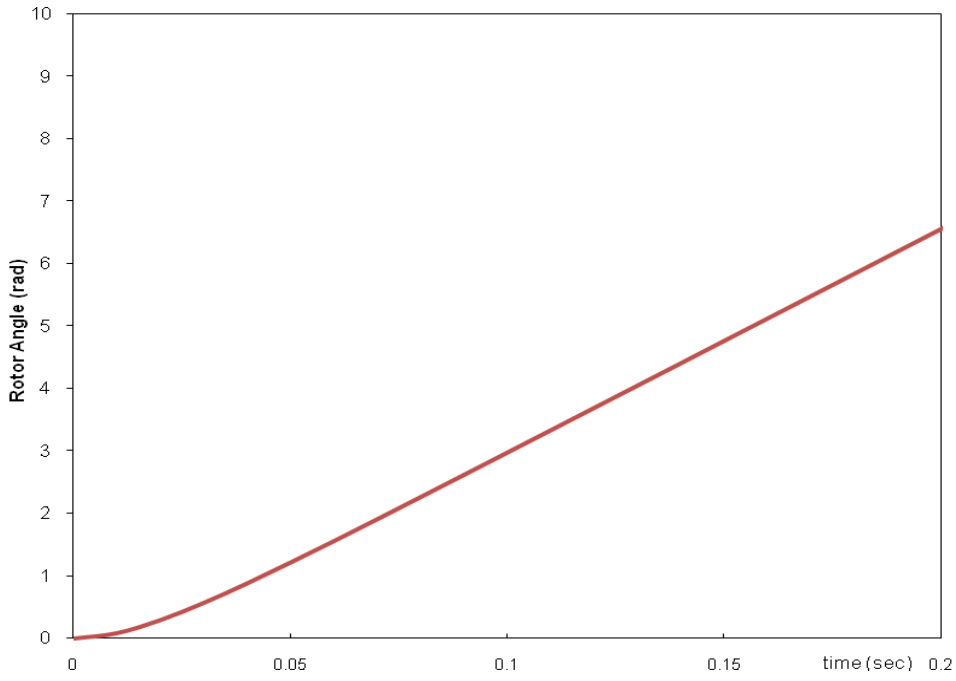

Figure 5.3 Open-loop responses for the DC motor system

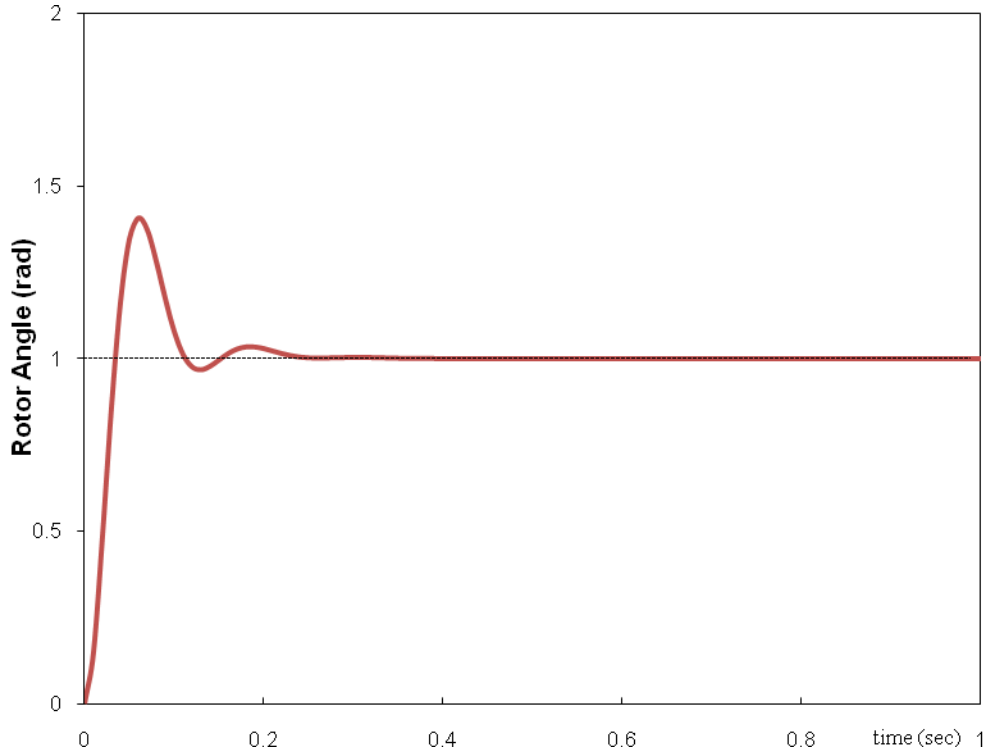

Figure 5.4 Closed-loop responses for the DC motor system

5.3 Modelling of the stepper motors

The stepper motor as shown in Figure 5.5 describes the two windings, B stepper motors. The characteristic equation of the motor is generally can be described as [33-34]

$$L_A \frac{di_A}{dt} = v_A - R_A i_A + K_m \omega \sin(N_r \theta)$$

$$L_B \frac{di_B}{dt} = v_B - R_B i_B + K_m \omega \cos(N_r \theta)$$

$$\tau = K_m (i_B \cos(N_r \theta) - i_A \sin(N_r \theta))$$

$$J \frac{d\omega}{dt} = \tau - B\omega \qquad (5.4)$$

where

i_A and i_B are the currents of the phase windings A and B.

R_A and R_B are the winding resistance which is assumed to be the same in the calculation

K_m is the motor torque constant

L_A and L_B are the winding inductance and assumed to be equal in the calculation

B is the rotational damping

J is the inertia.

N_r is the number of rotor teeth

τ is the motor torque

$\omega = d\theta / dt$

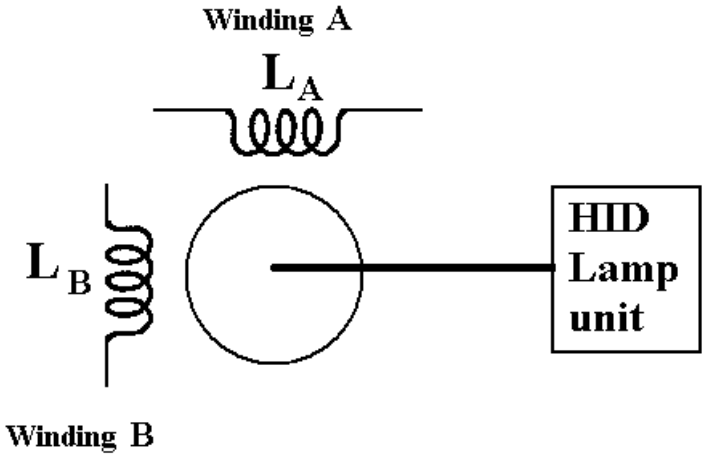

Fig 5.5 The Stepper motor

The motor parameter is described in Table 5.1. The model is shown in Fig 5.6 the mathlab model used for the study. The simulation result is shown in Fig 5.7.

Table 5.1: Stepper motor parameters

Parameters	Values
Number of phases	2
Winding resistance R	1Ω
Winding inductance, L	1.4mH
Step angle	1.7 degree
Inertia, J	3.2e-6 kgm^2
Winding rated voltage	6V
Motor torque constant K_m	0.028NmA^{-1}

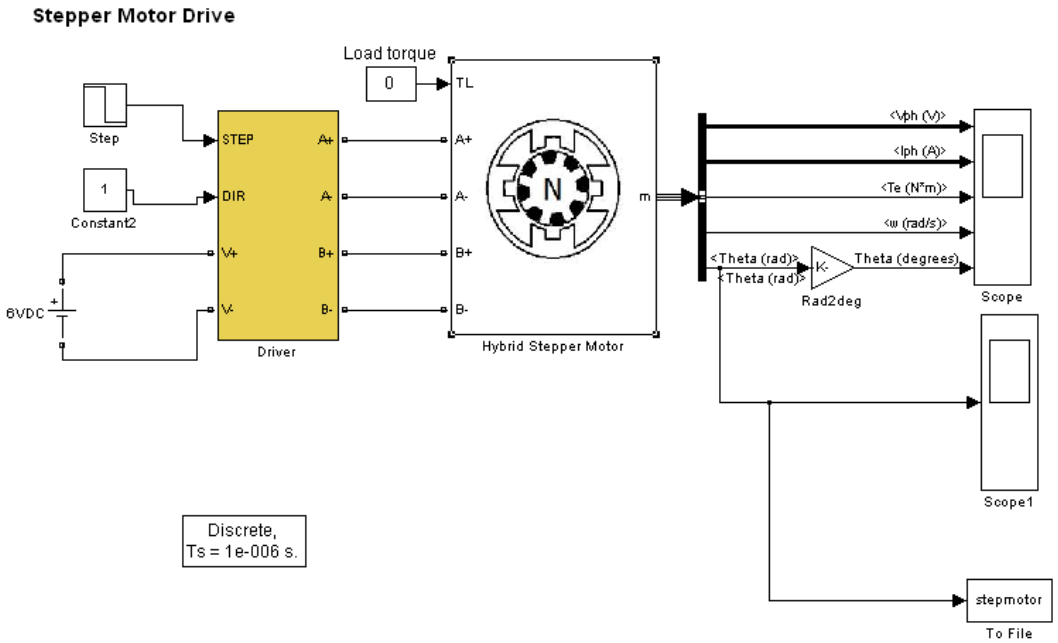

Figure 5.6 The Mathlab model for the stepper motor

The simulation result is shown in Figure 5.7. A test using 1 radian rotation is examined for the stepper motor to check the response of the stepper motor. It can be seen that the response time is 0.065 s.

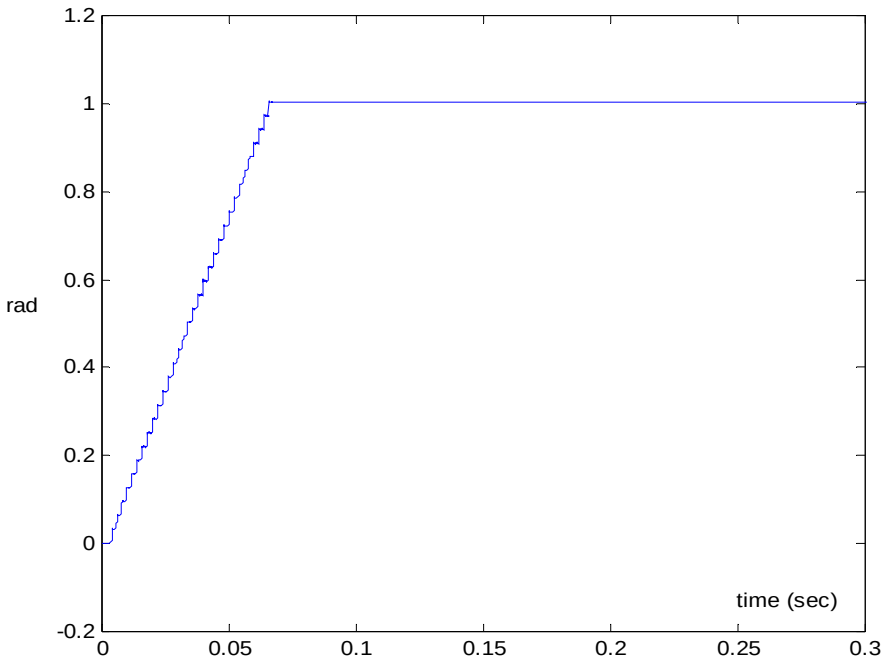

Figure 5.7 The stepper motor response under a rotation of 1 radian.

(1.8° /step, step rate 500/s)

5.4 Comparison between the DC drive and step motor drive

The aim of the adaptive lamp control is to provide the low cost and simple method control. The response time is important however, it is not a very essential for the rapid response because the normal driving time control is very slow as compared with the operation of the motor. Therefore even a rapid response will not affect the overall performance of the AFS. Comparing Fig 5.4 and Fig 5.7, it can be seen that the settle time for the DC motor is 0.25s whereas the settle time for the

stepper motor is only 0.065s. It is confirmed that for the present application, the stepper motor has advantages of a faster response, robust and lower cost. Table 6.1 shows the comparison of the performance of the two systems:

Table 5.2: Comparison between the step motor and DC motor

	Step motor	DC motor
Cost	$14	$20
Driver	$18	$15
Power driver	2 H-bridges	One H-bridge
Position control	Simple stepper control	Need PI control for position
Fault free	High fault tolerance	No
Response time Or a set of 1 rad	0.065s	0.25s
Overall comment	Lower cost Simple control Open loop is needed	Higher cost More complicated control PI control or closed loop position is needed

Although some study has shown that DC motor may has a better dynamic performance, the present motor with the same cost for DC motor and stepper motor shows that the DC motor has a poorer dynamic response.

5.5 Conclusion

In order to examine which motor is suitable for the AFS, the DC motor and the stepper motor have been used to study the response to the AFS. A model has been developed for the two motors. It is based on the first principle motor model and the torque equation. The model has been examined by programming in Matlab. It has been found that the response time for the DC motor is fast but the settle time is long whereas the stepper motor is very robust and the settle time is much shorter. To compare the cost, the total cost for a stepper motor and lower than the DC motor. No closed loop control is needed for the stepper motor. Therefore it has been recommended that stepper motor is selected for the AFS

Chapter 6.Analysis of System Functionality

6.1 Control method with the vehicle –vehicle distance

The test system is of a commercially available head lighting system consisting of separate high and low beam reflectors. The lighting system was already equipped with a stepper motor that controls the lever of the reflectors. Two sets of ultrasonic sensors were integrated in the system to collect the information on the distance of the oncoming vehicle. Light sensors were also used to detect the intensity of the ambient light as well as of the light from the vehicle in front.

The controller is designed to respond to conditions based on distance of the vehicle ahead and accordingly it responds to three stages given below.

Stage One

In stage one operation, the controller uses the signal from the ultrasonic sensor to switch between high and low beam lightings. This stage basically verifies the ability of the system to respond to the signals based on the distance of the objects ahead. An ultrasonic sensor having a range of over 50 m was used in the experiment. In Bi-Xenon Headlamp modules, the system will control the flap inside the reflectors which control the projection angle of reflects. A few tests have been conducted on this system. Two sensors were fitted on the front of the vehicle.

Comparison of signal will be made by the controller which can eliminate noise and increase the resolution.

Stage Two

In stage two, the lamp will be in low-beam and the controller basically controls the position of the lamp based on the inputs from the low-range sensor and the hall-effect sensors which detect the absolute pitch angle of the vehicle. The resolution of the low-range ultrasonic sensor is 0.1 m and the sampling period is 0.1 second. The noise is minimized by averaging the measurements every 0.5 second. The controller will adjust the angle of the low-beam in accordance with the measured average value.

In this set of parking aid sensor, the signal is collected from the display of the control unit. The display unit is driving by switch register 74VHC164. The signal from the sensor will go to the control unit and compare with the shift register. The shift register will control the MCU to decode the distance.

At this stage, a test for the angle of headlamp angle and distance has been carried out. The lamp has been adjusted according to the guidelines of the headlamp manufacturer specifications as shown in Fig 6.1..

The method for calculation of the level of headlamp beam is using the light

shadow as illustrated in Fig 6.2

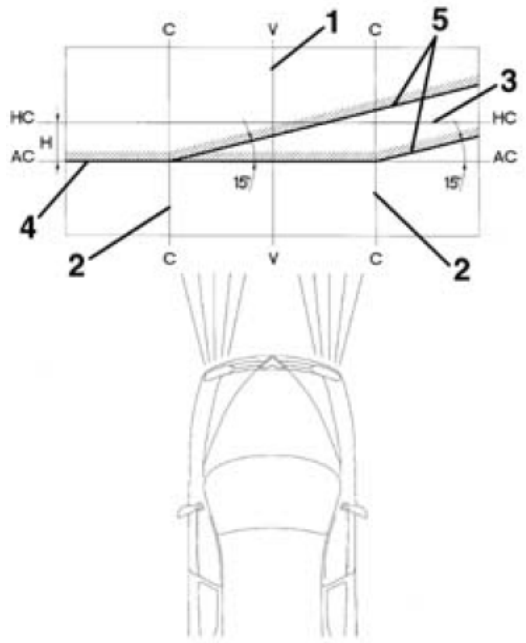	v –v: vertical, corresponding to the trace of vehicle plane of symmetry. c-c: traces of vertical planes passing through the reference centre of the light housing HC-HC: horizontal corresponding to the height from the ground of the reference centre for the light clusters. AC-AC: horizontal 10 cm below the line HC - HC. Lines inclined by 15° as illustrated in the diagram.

Figure 6.1 Headlamp Alignment Guidelines

The car must be placed on a flat surface and is perpendicular to a screen with an opaque surface 10 meters away.

Since there are physical limitations on adjusting the light 10 meters away from a perpendicular screen due to the limited space in the laboratory, the lamp shadow is adjusted in front of a screen with 6-meter displacement. The calculations are explained in the following text.

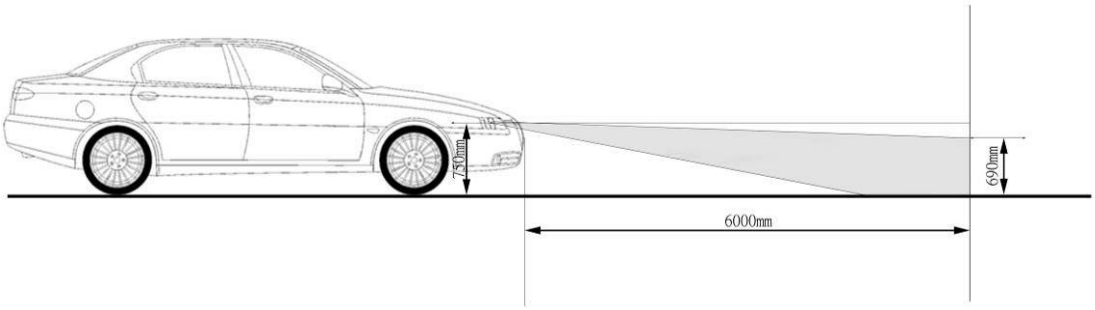

Figure 6.2: Testing Environment

In the test, the highest point of low beam level is 690mm at the distance of 6 meters as illustrated in Figure 6.2. Figure 6.3 shows the shadows projected by the headlamp such that its vertical level can be controlled by the proposed system.

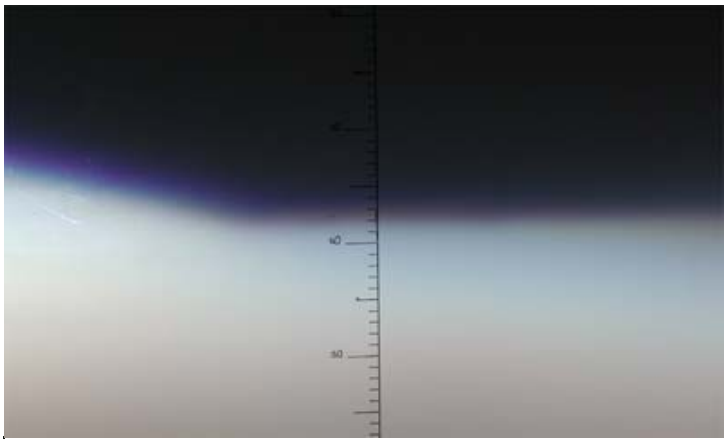

Figure 6.3: Marks for measured the headlamp shadow

6.2 The setup and measurement

Fig 6.4 shows the experimental rig. The motor is integrated inside the front-lamp. The unit is driven by 12V battery system and is obtained from a power supply for the laboratory test.

Figure 6.4: Testing Platform of Low Beam Levelling System

The sensors for this test were taken from a scaled down setting so that it can be conducted in the laboratory rather than using 50m test site. The sensor is calibrated for 10% sensor displacement so that now it can be used from 0-5m. For such test condition, a low cost parking ultrasonic sensor can be used.

The internal equivalent diagram of the angle relationship of the stepper motor and the actuation of the lamp unit can be illustrated as in Fig 6.5. The actual photos of the motor can be seen in Fig 6.6. The actuation of the lamp movement is done by a levelling system using a lever arm as shown in Fig 6.5. More description can be seen in next section.

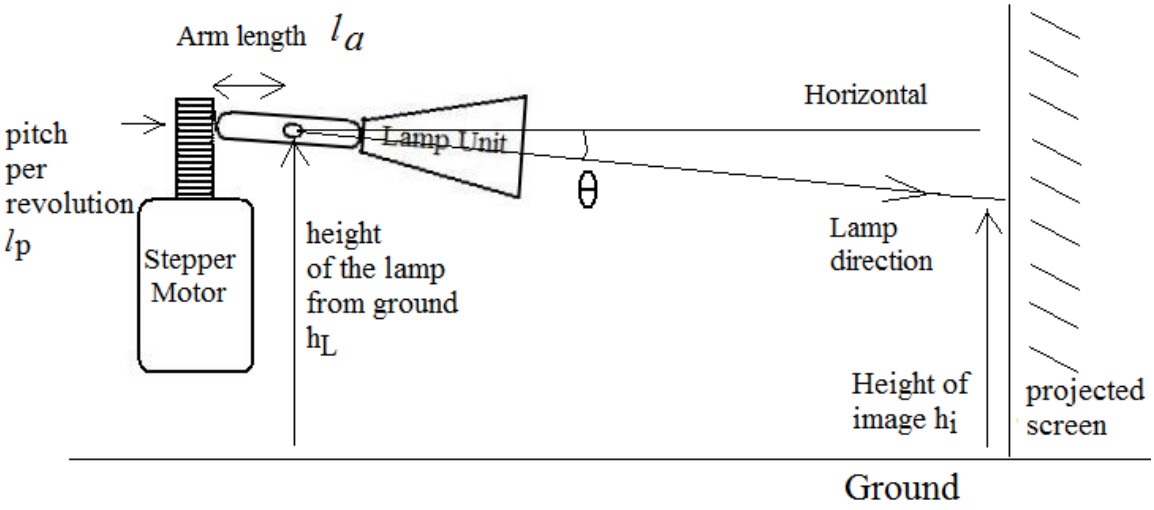

Figure 6.5: Illustration of how the stepper motor control the lamp direction

Now, height of the lamp h_L = 0.75m, the pitch per revolution l_p=1mm and arm length of the lamp actuator l_a=0.01m.

Fig 6.6 shows the relationship between the height of shadow and distance of the lamp from the screen. A is the distance of the lamp from the screen. B is the height of the projected image. It is the same as h_i.

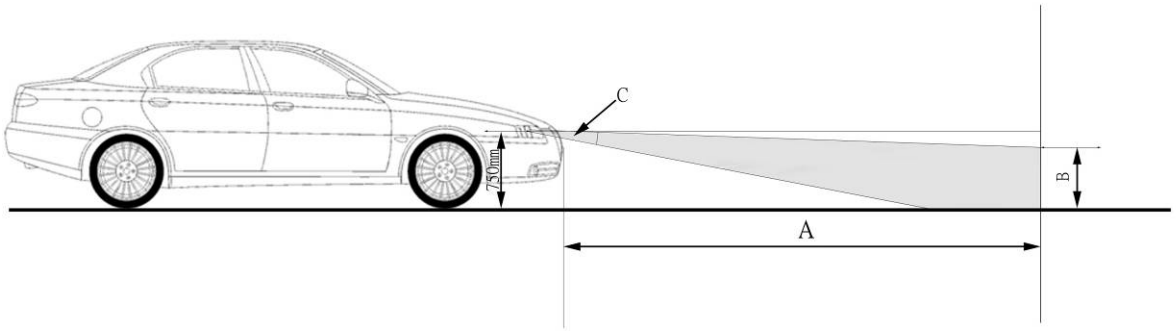

Fig 6.6: Annotation for short distance test

An obstacle is placed between the lamp and the projected screen in order to trigger the actuation of the ultrasonic sensor and hence the actuation of the stepper motor. The image height h_i was measured in the project screen. The angle of depression (dipped angle) θ is then calculated directly using tangent. The pitch movement l_p is calculated using l_a and tangent of θ. Since pitch per revolution of the motor is 1mm, therefore the revolution for each case is calculated.

The response time is difficult to measure. It is done by high speed camera to the image of the screen.

Table 6.1: Measurement of the angle of depression for laboratory test

Distance of obstacle (m)	Measured Image height h_i (m)	Angle dipped θ (rad)	Calculated Pitch movement l_p (m)	Revolution of motor	Measured Response time (s)
0.1	0.44	0.052	0.000517	0.517	0.23
0.5	0.44	0.052	0.000517	0.517	0.23
1.0	0.45	0.050	0.000500	0.500	0.22
1.5	0.49	0.043	0.000433	0.433	0.19
2.0	0.54	0.035	0.000350	0.350	0.16
2.5	0.59	0.027	0.000267	0.267	0.12

The data has been compared with the theoretical of the response time of the stepper motor is shown in Table 6.2.

Table 6.2: Comparison of the response time between measurement and motor model

Distance of obstacle (m)	Revolution of motor	Theoretical Response time (s)	Measured response time (s)
0.1	0.517	0.211	0.23
0.5	0.517	0.211	0.23
1.0	0.500	0.204	0.22
1.5	0.433	0.177	0.19
2.0	0.350	0.143	0.16
2.5	0.267	0.109	0.12

6.3 The measurement of H-bridge

The operation principle of levelling system is done by the light angle actuator. The actuator includes a bi-polar stepper motor and an arm.

Figure 6.7: Bi-polar stepper motor

When the motor rotates clockwise, the arm will be extended and the light pointed upwards. The light pointed downwards while the motor rotates in anti-clockwise direction. The bi-polar stepper motor (Fig 6.7) is controlled by two

H-bridge controllers and a micro-processor generates pulses to control the H-bridge controllers. In initial stage, the stepper motor will be driven anti-clockwise for 200 turns to ensure the arm is fully contracted. After a signal is received, the motor turns to a preset position by counting the pulse. The light angle actuator moves upwards and downwards according to the incoming signal. The system is in open-looped and no feedback is required because the torque required is small. In such case, the motor is assumed that no slip of position occurs during low speed operation (around 60-120 rpm). Fig 6.8 shows the measured signal from the MCU that is square pulse to excite the motor. Fig 6.9 shows the H-bridge voltage signals. Fig 6.10 shows the winding voltage of the motors. It can be seen that all the signals for square wave and the control and voltage drive of the motor are therefore simple.

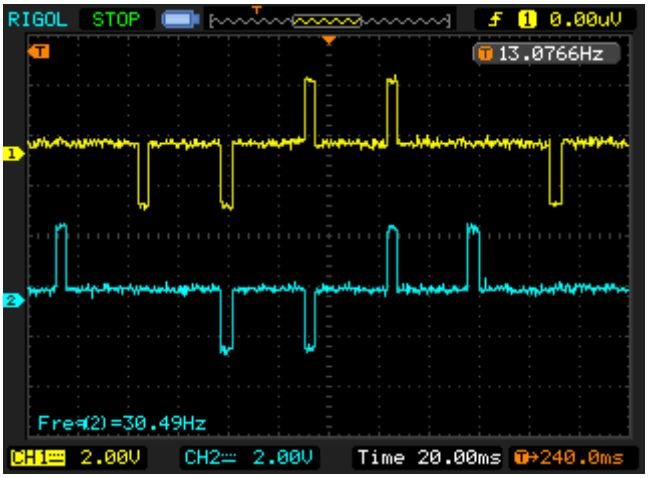

Figure 6.8: Input Signal from MCU to Driver
Channel 1: Input signal to H-bridge for winding A (4V/div)
Channel 2: Input signal to H-bridge for winding B (4V/div)

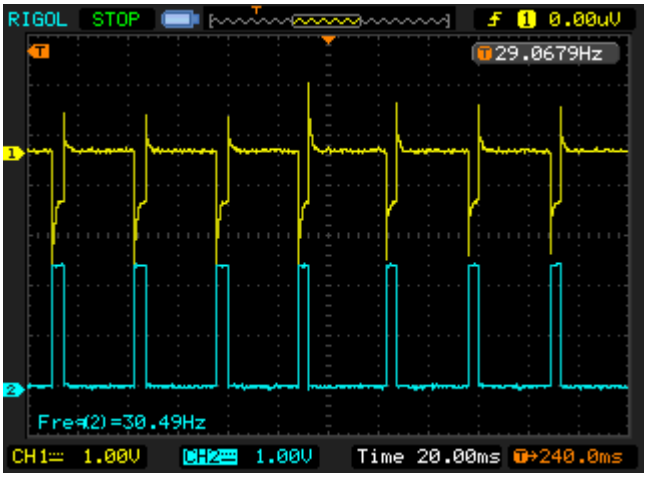

Figure 6.9: Comparison of output versus input signal of H-bridge
Channel 1: Output signal from H-bridge for winding A (4V/div)
Channel 2: Input signal to H-bridge for winding A (2V/div)

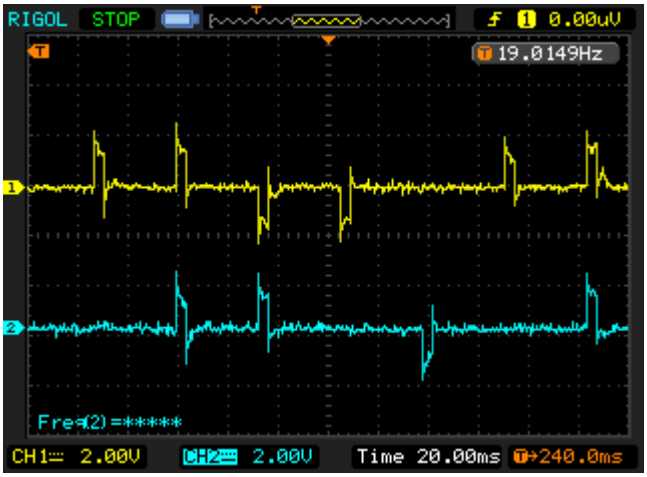

Figure 6.10: Output Signal of windings
Channel 1: Output signal from H-bridge for winding A (4V/div)
Channel 2: Output signal from H-bridge for winding B (4V/div)

The slip will occur when the stepper motor speed increases. Therefore careful design has been used to ensure that the speed of the stepper motor will not beyond the limited. Experiment test has found that the speed is limited less than 300 rpm. In this case, a simple open loop control is needed rather than a position feedback is used. This can reduce the overall cost of the system.

Stage Three

In stage three the controller initiates dimming control upon detection of vehicles nearby. The distance detection is provided by the ultrasonic sensor while the command for the dimming is provided by the light sensors which will detect any reflected light from the vehicles in the front. The controller will detect this output and sends a signal to the processor in the HID ballast for dimming operation. The processor then operates the lamp at low power causing dimming of the lamp. The present design has not implemented the dimming control as it is beyond the scope of the project and will be considered for future work.

6.4 Response of the Step motor control

The step motor can provide a very fast control against the control signal to the motor. To control the lamp for the turn of certain angle can be illustrated in Fig 6.11. The diagram shows that the response time and is derived from the experiment in Section 6.2. It can be seen that the response time of stepper motor is high for AFS application.

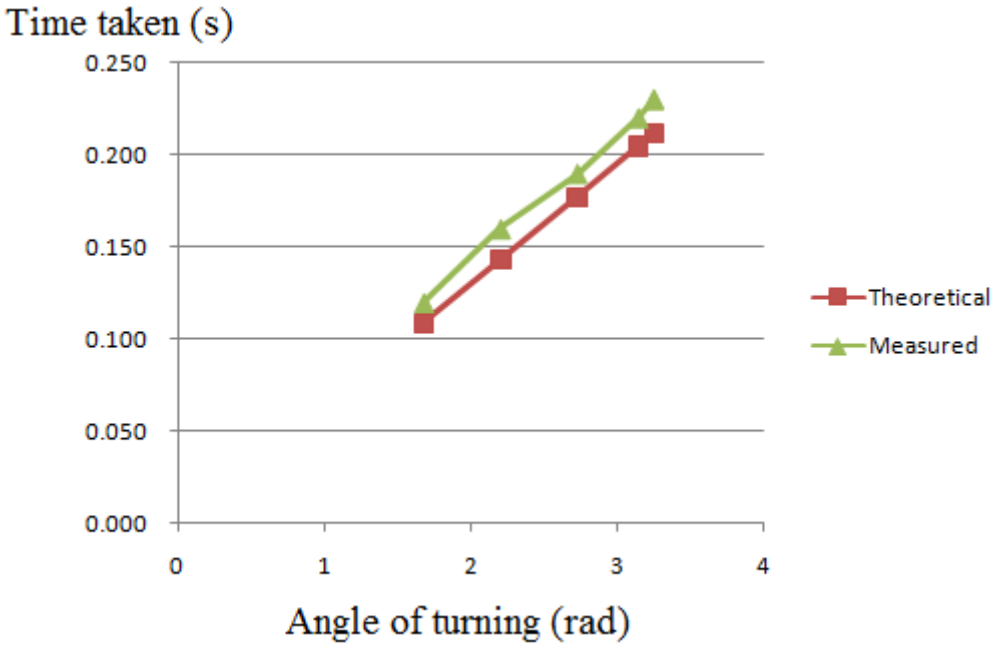

Figure 6.11 Illustration of the speed of the motor.

6.5 Summary

This section describes a control implementation of the system. The control of the vertical level control with the vehicle to vehicle displacement control is explained. The two coil control for the stepper-motor is explained. The system has been implemented in the front-lamp. The control waveforms are shown. The response time of the system is fast and can able to provide maximum angle of depression within 0.25 s. The test confirms the functionality of the system built.

Chapter 7. Conclusion

7.1 Conclusion of the project

Automatic Headlamp Control proves to be effective on minimization of the chance of glaring other road users in the dark. This improves the effectiveness of headlamp by increasing the light projected area. The project has conducted works on the low and high beam control and examined the operation under different road conditions.

The Simulink model has been presented to examine the logic flow of different parts of the Advanced Headlamp Control System. This simulation provides a functional analysis of our design ideas before building a physical model. Time of developing a new system by using simulation can reduce time and failure rate. Simulation results of 3 different cases have been provided in details.

The comparison between the DC motor and stepper motor has been conducted. A model for the DC model and stepper motor have been developed and used for the investigation of the response. It has been found that for the present application, the stepper model has a better response characteristic than the DC motor. It is also lower cost as a whole. Therefore stepper motor has been selected for the project. For information, the commercial market is now using

stepper motor for similar lighting control application.

An experimental prototype has been built and tested. Through the experiment, the motor installed in the headlamp has confirmed to have a very quick and accurate response to cope with the sudden change of the road environment. Ultrasonic sensors have been tested in the experiment. The short range ultrasonic sensor provides an accurate reading of distance between the vehicle and obstacles. The long range sensor provides a stable reading without interference by other noises. On the road, the environment changes a lot. Sensors must be installed for checking all the environment condition continuously.

The prevention of EMI is also very important in this project. Switched Capacitor Resonant Power Supply is being used for this system. The converter has been developed based on simple gate drive and therefore the circuit is simple. The analysis for the circuit has been conducted. The circuit has been built and tested for the AFS. It has a good efficiency on reducing the voltage from 12V to 6V. The EMI is very low comparing with other types of Power Supply. Furthermore, it has an advantage of light weight and low production cost due to its simple design.

In summary, the project has examined the beam control for AFS and different cases analysis has been conducted and implemented in a practical system. A low

EMI power supply is developed to integrate with the overall system. The AFS has been implemented in an electric vehicle EV4. The vehicle is designed to be all electric and with 4kW motor drive system. The vehicle has been demonstrated to be good performance.

7.2 Further works

This new system has proved to increase the area of headlamp projection without glaring the other road users. However, this new system still requires improvement. An Advanced Adaptive Front lamp System (AAFS) should be developed to compensate the weakness of my new system. AAFS includes the function of Adaptive Front lamp System (AFS) and the presented work Advanced Headlamp control system. The Advanced headlamp works well on the road which is wide and straight but not helping a lot in those narrow and twisty roads. The reason is the Advanced Headlamp Control cannot adjust the direction according to the directions of the road.

AFS has the ability of changing the direction of headlamp. The first AFS system was appeared in 1950s. The system was first used by Citroen, a French manufacturer. Their model Citroen DS equipped with a mechanically linked AFS system. The lamps in the front will change their direction according to the turning of the steering. Due to the outdated vehicle legislation in many countries, the number of cars selling with AFS equipped is very low. Due to its unpopularity, the manufacturers finally dropped out this features from their production line until 1990s. The revision of national vehicle regulations allows AFS headlamp legally installed on vehicles.

The Advanced AFS must have a prediction of the road direction ahead. The

headlamp should be turning before the car actually turns. In some recent findings, the headlamp was guided by steering wheel as well as GPS system. Unfortunately, the functionality is limited when the function of GPS is interfered by the surrounding area.

Although the experimental results of this project are quite satisfactory, further work can be done to make it better. In the experiment, we proved the relationship of the ultrasonic senor (distance) to the headlamp angle. However, the test has been scaled down because of the sensor limitation. In the next step, a longer range sensor which obtains the same range as this system is designed should be used to do a real-life test on this system.

Since EMI problem is very important on vehicle, the EMI test should be carried out for the whole unit in order to avoid interference to the system.

Chapter A. Appendix

A.1 Introduction

Headlamp is one of the key components in the vehicle. An efficient Headlamp can help to reduce energy consumption in Fuel powered vehicles as well as electric vehicles. Since the design of this headlamp control unit has the feature of low power consumption and high power efficient, it benefits the overall range of the electric vehicles. This chapter describes the design of the electric vehicles and the implementation of the AFS to the vehicle.

A.2 Design of Electric Vehicles

In an Electric Vehicle, the major electronic components are: Batteries, Motor, Motor Controller and battery charger. To design an Electric Vehicle, First we need to identify the major function of that vehicle. There are different types of EV in the market. They are classified as Electric Neighbourhood Vehicles (Golf Kart), Private Electric Road Vehicles and Commercial Electric Road Vehicles.

For Electric Neighbourhood Vehicle, the Overall size is generally smaller and the weight which is less than 500kg. The payloads are generally lower. Also, they are not permitted to drive on public roads. In the Motor Control System, the design is very

simple. The average voltage and current are about 24-48 Volts and 2-10kWh. Its average speed are not more than 40km/h. inside the vehicle, it does not have any high power consumption devices such as Air Conditioning System and Heated Seats. Therefore the requirement of power from the drivetrain is very low..

For Road Private Vehicles, it is designed for longer range. The gross weight is around 1,000kg – 1,500kg. The motor drives installed on the car are usually high voltage AC induction motor, mostly three-phase. The average voltage is about 110-300V and the power output is around 20-80 kilo-watt. Apart from motor drives, air-conditioner, heated seats and power windows are also consuming lots of power from the batteries.

Road Commercial Vehicle, which also designed for long range with heavy goods or large number of passengers. The Gross Weight is about 2,000kg – 4,000kg. The power-train should be capable of heavy load. High Voltage and High Power motor will be used with the average of 400VAC and >60 kilowatt. Auxiliary Electric Appliances are also installed on these vehicles such as Air Conditioner and Cargo Lifter.

A.3 Vehicle packaging

A.3.1 Motor Drive

The conventional motors including the DC motor, induction motor, DC brushless

and switched-reluctance considered for electric vehicle propulsion motor. On new generation of low power Electric Vehicle, DC brushless drive as shown in Fig 8.1 will be preferable because of its brushless purpose. The advantage is ease to maintain. Users are not required to renew the brush. However, the cost for DC Brushless Drive is higher than brushed DC drives. Beside the Brushless DC Drive, Separately-exited DC Drive is also common because of low cost. No extra components are required in this motor for regenerative braking. For small town car and because of the range is short, DC motor will be used for the design.

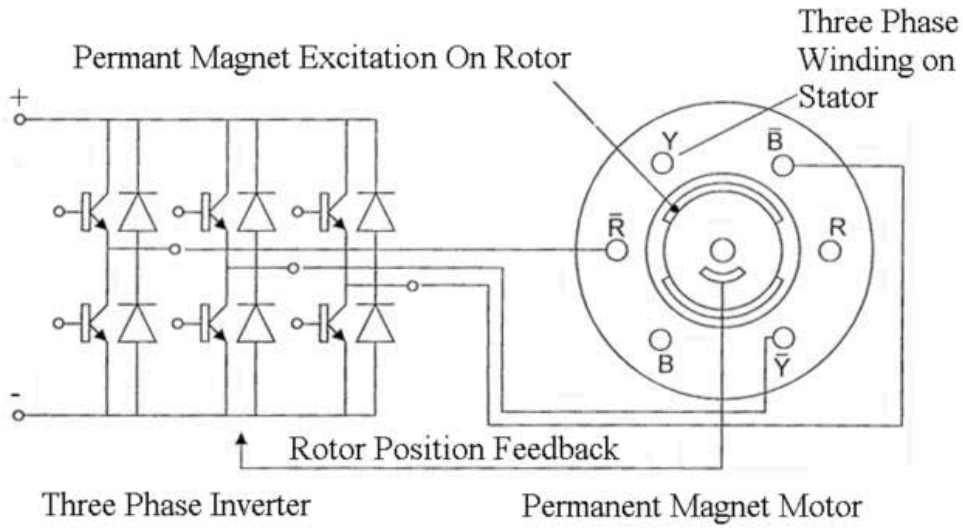

Figure A.1: Components of DC Brushless Motor Drive

Switched Reluctance (SR) Motor is the motor which mounted phase coils diametrically opposite stator poles as shown in Fig 8.2. The rotor is made of silicon iron without winding. The energised phase will lead to the rotor moving into alignment with

the stator poles. SR Motor gives better torque. In the diagram below, that shows a four-phase SR Motor. Five- and six-phase motors are also exists in the market. It can offer better torque ripple reduction compared with four-phase and three-phase. Although the cost of the motor is theoretical low because of the simple design, however, because of the market share is still low as compared with induction or DC motor, the total cost of the motor and drive is still very expensive.

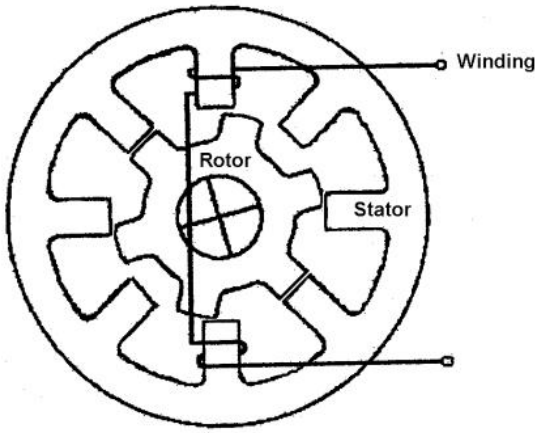

Figure A.2: An 8/6 Switched Reluctance Motor

For the present design of an Electric Neighbourhood Vehicle, the major design critical is low cost, short range, and low speed. Finally a DC motor is selected.

A.3.2 Battery

Lead Acid Batteries are the most common batteries used in low price and low power Electric Vehicles. The cost for these batteries is comparatively low. However, the Power

Density is not as good as Nickel Metal Hydride (NiMH) and Lithium-ion (Li-ion). Also, the charging cycles are the worst among three. In the market, there are deep cycle batteries with provide longer service life charging cycles. Unfortunately, those batteries are larger, heavier than non deep cycle one.

Nickel Metal Hydride Batteries has higher Energy and Power density as compared with Lead Acid Batteries. Unlike Lead Acid Batteries, it must be sealed due to the inherent characteristics of the system. Its lower cell voltage means higher number of cells required than Lead Acid Batteries. The cost is higher than Lead Acid Batteries but it has longer service life cycles

Table A.1 Comparison between 3 types of batteries

Properties	Lead Acid	NiMH	Li-ion
Cell Voltage	2 Volt	1.2 Volt	3–4 Volt
Energy Density	25–30Wh/kg	35–80 Wh/kg	60–150 Wh/kg
Energy Efficiency	75–80%	60–85%	85–90%
Power Density	100–200 W/kg	100–1000Wh/kg	300–1,500W/kg
Service Life in Cycles	600 - 900	Over 2,000	Over 1,000
Operating Temp.	10–55℃	-20–55℃	-10–60℃

Lithium Batteries have highest Energy and Power Density among three. Its working temperature is slightly higher than others. The voltage of each cell can be as high as 4Volt. However, the cost for using Lithium Batteries is high. There is also a shortage supply

of the high power Li-ion battery. The supply of the Li-ion is inconsistent and the lead time is long.

In Electric Vehicles, there are 12V, 24V, 42V 48V, 140V, 280V, or even higher voltage systems. Light weight electric vehicles such as Golf Kart with less than 4kW usually choose 48Volt or less system. The reason is that the system lower than 48V generally not requiring to comply with some of the safety regulation standards. Due to low voltage used, the current for driving the motor is very high. Therefore there are higher losses from the cable, hence thick wire should be used. Thicker wire will increase the overall weight of the vehicle and cost. On High Voltage System, it is usually designed for Private Vehicle and Commercial Vehicles. Thinner wires can be used due to lower current. It benefits weight too.

For the present design of an Electric Neighbourhood Vehicle, 48V system is selected between of the lower power rating of the driving system. The battery is selected to be deep-cycle lead-acid type in order to reduce the total cost.

A.4 Design equation for EV

Car Dynamics

In the process of designing an Electric Vehicle, series of calculations have been done before assembling the running prototype.

The calculation is based on the PolyU EV3 requirement. The initial specifications are:

PolyU EV3 – Total Weight: 590kg; Coefficient of Drag: C_d=0.25; Headwind: 1m/s; Motor Power: 4kW; Largest Cross Section Area: 1.624m^2, Battery: 12V 4x100A

The above data is very much comparable to a Golf-Kart and also lower requirement than a private car. For reference the general data for Golf-Kart and private car are given below:

Golf Kart – Total Weight: 500kg; Coefficient of Drag: C_d=0.35; Headwind: 0m/s; Motor Power: 2kW; Largest Cross Section Area: 1.5m^2, Battery: 12V 4x100A

Private Car– Total Weight: 1500kg; Coefficient of Drag: C_d=0.35; Headwind: 0m/s; Motor Power: 20kW; Largest Cross Section Area: 2m^2; Battery: 12V, 8x100A

Motive Force.

$$F = \frac{M \cdot i}{r} \cdot \eta \qquad \text{(A.1)}$$

where:

F = Motive Force (kg/h)

M = Motor Torque (Nm)

i = Transmission Ratio

η= Drivetrain efficiency

r = Wheel radius (m)

Climbing resistance and downgrade force.

$$F_{st} = G \cdot \sin\alpha$$
$$F_{st} = m \cdot g \cdot \sin\alpha \qquad \text{(A.2)}$$
$$P_{st} = F_{st} \cdot \upsilon$$

where:

F_{st}= Climbing Resistance (kW)

G= Weight (N)

m=Vehicle mass (kg)

g= Gravitational Acceleration (9.81m/s^2)

v=Vehicle Speed (m/s)

α= Gradient Angle (rad)

Aerodynamic Drag

$$F_D = 0.5\rho C_d A(v + v_o)^2 \quad \text{(A.3)}$$

where

F_D=Aerodynamic Drag (N)

ρ=Air Density (kg/m^3)

C_d= Coefficient of Drag (N/m^2)

A = Largest Cross Section of the Vehicle (m^2)

v=Vehicle Speed (m/s)

v_o=Headwind Speed (m/s)

Rolling Resistance

$$F_{Ro} = f \cdot m \cdot g \cdot \cos\alpha \quad \text{(A.4)}$$

where

F_{Ro}= Aerodynamic Drag

f= Coefficient of Rolling resistance

m=Vehicle mass

g= Gravitational Acceleration (9.81m/s^2)

α= Gradient Angle

Total Running Resistance

$$F_W = F_{RO} + F_D + F_{st} \quad \text{(A.5)}$$

$$P_w = F_w v$$

where

F_W= Running Resistance (N)

F_{RO}= Aerodynamic Drag (N)

F_L=Aerodynamic Drag (N)

F_{st}= Climbing Resistance (N)

v= vehicle speed (m/s)

P_W= Running Power Resistance in kW

After all these calculations, the value of Motive Force should be higher than Total Running Resistance. Otherwise the vehicle is being able to move.

The design of the vehicle is based on the specification as shown in Section 8.5.

The case for flat road and inclined road with maximum 5 degree was used for the

calculation. Table A.2 shows the calculation:

Table A.2 The calculation of the total force for the vehicle design

Road type	**Symbol**	**Inclined road**	**Flat road**	**Unit**
Vehicle mass	m	590	590	kg
Maximum Gradient	α	5	0	degree
Climbing force	$\mathbf{F_{st}}$	**700**	**0**	**N**
Coeff. of Drag	C_d	0.25	0.25	
Cross-sectional Area	A	1.624	1.624	m^2
Head wind speed	v_o	1	1	m/s
Dragging force	$\mathbf{F_d}$	**1.4**	**103.5**	**N**
Rolling force	$\mathbf{F_{ro}}$	**57.6**	**57.8**	**N**
Total Running Resistance	$\mathbf{F_W}$	**759**	**161.3**	**N**
Peak Vehicle Speed	v	5	70	km/h

The above total running resistance force defined the need for the motor drives.

Table A.3 The design of the motor and drive system

Power	P	4	kW
Max Torque	T	38	Nm
Transmission Ratio	i	7.5	
Drivetrain Efficiency	η	80%	
Wheel Radius	r	0.3	m

For the total power of 4kW in the drive, The lighting system accounts for 35W lamp

power and 2.5W driver power for each lamp. With 80% efficiency of the ballast, the power for each lamp is 46.2W. Each lamp unit has two HID lamps for Lo and High beams. The total power for the AFS is therefore 185W. This is equivalent to near 5% of the motor power.

A.5 Technical Specification of PolyU EV3

Performance:

Maximum Speed:	70 km/h at GVW on Flat Roads
Maximum Range:	80 km at GVW on Flat Roads
Maximum Gradient:	~5 degree at GVW

Weights and Dimensions:

Body and Finish:	Painted Fibreglass Body Panels
Steering:	Rack-and-Pinion,
Turning Radius:	4.2 m
Number of Seats:	2
Unladen Weight:	440 kg (without a driver, with batteries)
Maximum Safe Load:	150 kg
Total Authorized Laden Weight:	590 kg
Length:	2,653 mm
Width:	1,396 mm
Height:	1,446 mm
Wheel Base:	1,691 mm
Track:	Front: 1,173 mm - Rear: 1,227
Ground Clearance:	100 mm

Technical Specifications:

Batteries:

Type:	Lead AGM Deep Cycle Batteries, maintenance free
Number of Batteries in Pack:	4
Batteries pack voltage:	48V
Pack Tension:	100 Ah
Pack Capacity:	4.8kWh

Onboard Battery Charger:

Domestic Electric Supply:	190 - 255V AC, 16A
Charging Power:	2100 W
Recharge Time:	8 – 10 hours (quick charge: 3 hours)
Charger:	48V DC

Motorization:

Motor Type:	48V DC Electric Motor with Serial Excitation
Maximum Power:	4kW
Transmission:	Electronic Controlled Single Speed Automatic with differential (forward, reverse, neutral)
Batteries Location:	Front of Vehicle
Type of Drive:	Rear Wheel Drive
Tyres and Wheels:	13” Aluminium Alloy Wheels (165 / R13)
Auxiliary Equipment:	Powered by a 12V 18Ah Lead AGM battery re-charged by a DC/DC Converter
Speed Control:	Electronic Controller with Regenerative Brake to increase drive range
Chassis:	Steel Tubular Space Frame with Roof Frame

Suspension:

Type:	Independent on All Wheels
Front:	McPherson Type with Coil Springs and Dampers
Rear:	Trailing Arm Type with Coil Springs and Dampers

Braking System:

Type of braking:	Dual Circuit Hydraulic Braking System
Front:	209 mm diameter brake discs
Rear:	209 mm diameter brake discs
Parking Brakes:	Mechanical on Rear Axle

The chassis of the electric vehicle PolyU EV3 is shown in Figure A.3 It can be seen that the basic mounting of the electric unit including the air-conditioning system, motor and the wheel. Fig 8.4 shows the motor used and its differential gear that is to drive the two rear wheels.

Figure A.3 The chassis of PolyU EV3

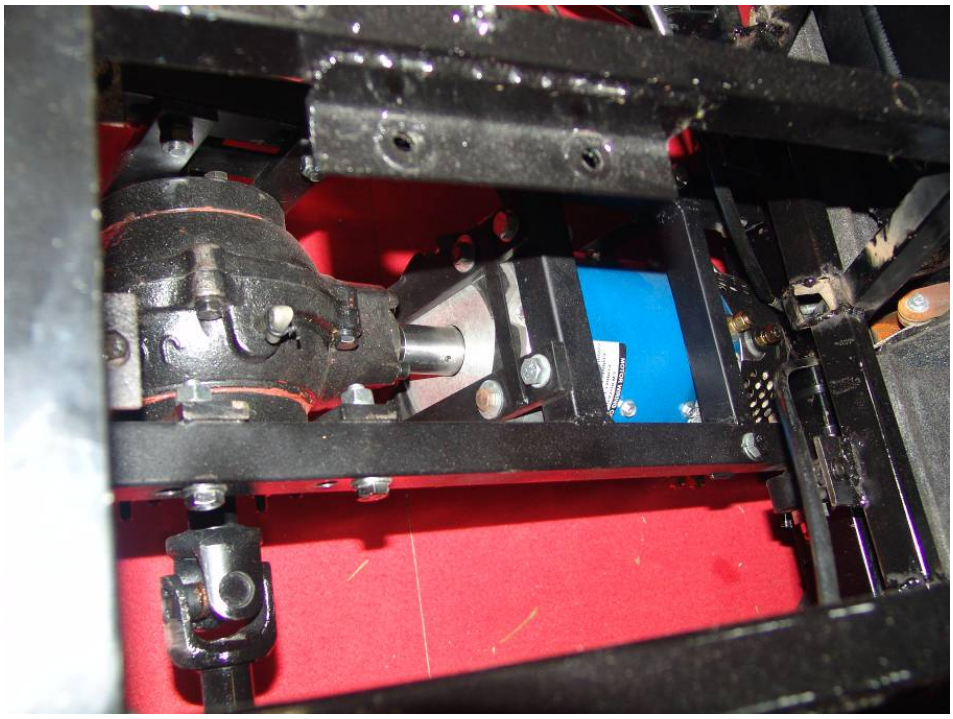

Figure A.4 The motor and differential gear

This is a direct drive from the motor to the differential gear. The design can reduce

the loss as compared with the conventional design of chain drive. The differential gear is a 7.5:1 unit that provides the high torque and the speed differential during cornering.

Fig 8.5 shows the implementation work conducted for the EV3. The speedometer, control electronics and the electric system were being installed.

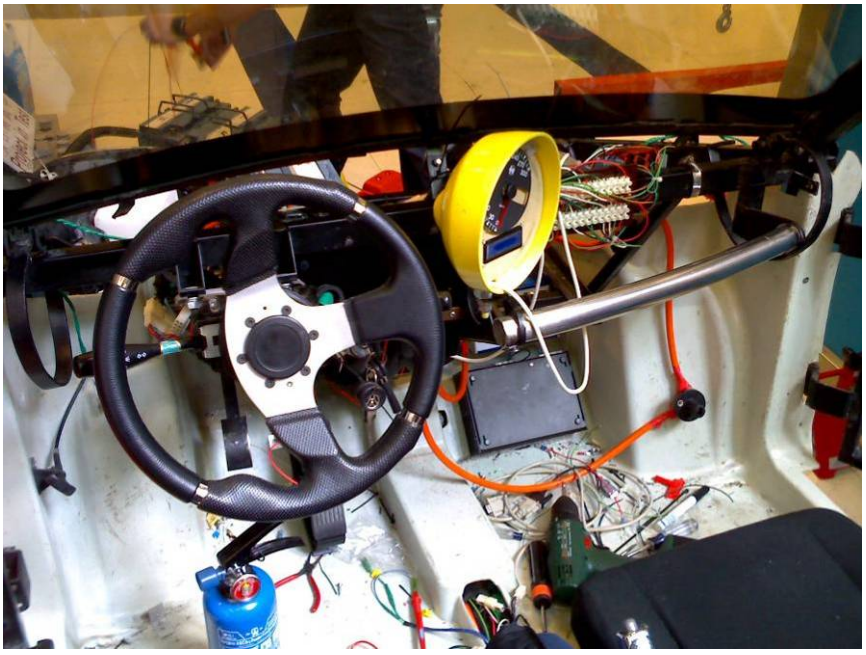

Figure A.5, The installation work conducted for the EV3

The system is now all electric with the self-developed work in motor drive, electric system and lighting system. Figs 8.6 and 8.7 show the finished EV3.

Figure A.6 The PolyU EV3 rear view

Figure A.7 The PolyU EV3 front view

Another model EV4 is also developed. This is identical to EV3 with installation of the latest lighting system.

Figure A.8 shows the implementation of the HID lamp system. The four HID ballasts in a metal package are attached to the chassis as shown. The wire for the ballast to the lamp is made short in order to reduce the EMI. The ballast is connected to both high beam and low beam lamps. The motion control is to actuate the low beam HID. The system has been found working successfully. Figure A.9 shows the rear lamp which is developed using LED. The LED provides alternative method to lighting system and has provided high performance illumination.

Figure A.8 HID installed to the PolyU EV4.

Figure A.9 LED rear lighting installed in PolyU EV4

Figure A.10: The finish model of the EV4

Figure A.10 shows the finished model of EV4. The vehicle is all electric and with the above said specification. The front-lighting system based on the AFS has been developed and working satisfactory.

A.6 Conclusion

Designing a good electric vehicle is not an easy task. We need to fully understand the need of that vehicle and choose the right vehicle package and components in order to maximize its overall efficiency. Electric Vehicles with complicated electronic power

controls will be the trend of future electric vehicles.

The town car (Neighbourhood Vehicle) versions of an Electric vehicle has been studied, designed and constructed. The electrical interfacing, battery size, motor size and the users' requirement have been examined. This town car is based on Golf kart specification and has been tested and the starting, running and braking characteristic has been examined. The characteristics will then be used as a base to design the other town car or private vehicle. From the experience and the testing for the vehicle for the last 12 months, the development of a power efficient and effective headlamp control unit for a town car can effectively reduce the power consumption and improve the quality of illumination.

References

[1] H.J.Chiu, H.M.Huang, and Y.K.Lo, C.H.Li, “High-Frequency Dimmable Electronic Ballast for HID Lamps”, IEEE Trans. Power Electron., vol. 21, no. 5, pp. 1452-1458, Sept. 2006

[2] K.C.Lee and H.C.Bo, “Design and analysis of automotive high intensity discharge lamp ballast using micro controller unit”, IEEE Trans. Power Electron., vol. 18, no. 6, pp. 1356-1364, Nov. 2003.

[3] D.H.Wang, K.W.E.Cheng, B.P.Divakar, P.Dong, W.W.Chan, X.D.Xue, K.Ding, Y.B.Che and C.D.Xu, “Development of an Automotive HID Electronic Ballast Based Microprocessor”, Proc. ICPESA ’06, pp. 229-233, 12-14 Nov. 2006.

[4] C.M.Huang, T.J.Liang, R.L.Lin and J.F.Chen, “Constant power control circuit for HID electronic ballast”, Proc. IAS 2005, vol. 2, pp. 1193-1197, 2-6 Oct. 2005.

[5] F.S.Dos Reis, J.C.Lima, R.Tonkoski Jr, C.G.Dantas, T.Suzuki, F.Martinazzo and L.A.Godinho, “Electronic Ballast Design System”, Proc. IECON ’03, vol. 1, pp. 800-805, 2-6 Nov. 2003.

[6] K.F.Kwok, K.W.E.Cheng and P.Dong, “General study for the design of HID ballasts”, Proc. ICPESA '06, pp. 182-185, 12-14 Nov. 2006.

[7] P.Flesch and M.Neiger, “Numerical investigation of time-dependent electrode-plasma interaction in commercial HID lamps”, IEEE Trans. Plasma Science, vol. 33, no. 2, Part 1, pp. 508-509, Apr 2005.

[8] M.Gulko and S.Ben-Yaakov, “A MHz electronic ballast for automotive-type HID lamps”, Proc PESC ’97, vol. 1, pp. 39-45, 22-27 June 1997.

[9] N.Aoike, M.Hoshino and A.Iwabuchi, “Automotive HID headlamps producing compack electronic ballasts using power ICs”, IEEE Industry Applications Magazine, vol. 8, no. 1, pp. 37-41, Jan.-Feb. 2002.

[10] K.Ishiguri, M.Hoshino, A.Iwabuchi and N.Aoike, “Power IC of electronic ballast for automotive HID lamp”, Conf. Record IEEE Industry Applications, vol. 5, pp. 3388-3393, 8-12 Oct. 2000.

[11] B.Wang and X.Xiao, “Application of multi-mode control strategy in the automotive HID headlight systems” Proc. WCICA 2008, pp. 8064-8068, 25-27 June 2008.

[12] Y.Tsutomu, O.H.Masto, S. Toshihisa, K. Gunji and K Takeshi, “Characteristics of ballast for HID lamp with single-ended resonant-type inverter circuit using leakage inductance of transformer,” Proc. PEDS, pp. 246-250, June 1995.

[13] J.M. Alonso, C.Blanco E. Lopez, A.J. Calleja and M. Rico, “Analysis, design and optimization of the LCC resonant inverter as a high-intensity discharge lamp ballast,” IEEE Trans. Power Electron., Vol. PE-3, pp. 573-585, May 1988.

[14] M. Gulko, S. ben-Yaakov and A. Giter, “Current sourcing push pull parallel-resonance inverter (CS-PRI): Theory and applications as a discharge lamp driver,” IEEE Trans. Power Electron., Vol.41, pp. 285-291, June 1994.
\

[15] S. ben-Yaakov, M. Gulkho and A. Giter, “The simplest electronic ballast for HID lamps,” IEEE Trans. Ind. Electron.,, Vol.41, pp. 634-640, Sept, 1996.

[16] T. Hacibekir, S. Karaman, E. Kural, E.S. Ozturk, M. Decmirci and B.A Guvenc, “Adaptive Headlight System Design Using Hardware-In-The-Loop Simulation”, IEEE International Conference Control Applications, 2006, S.Y.R. Hui and H. Chung, “Dimming control of electronic ballasts,” U.S. patent 6486651, Nov. 26, 2002.

[17] J. Roslak and J. Wallaschek, “Active lighting systems for improved road safety.”, Intelligent Vehicles Symposium, 2004 IEEE, pp. 682-685, 14-17 June 2004.

[18] S.Y.R. Hui, H. Chung, L.M. Lee and Y. Ho, “An electronic ballast with wide dimming range, Low EMI and high power factor,” *IEEE Trans. Power Electron.,* Vol 16, pp. 465-472, July 2001.

[19] S.Y.R. Hui and H. Chung, “Dimming control of electronic ballasts,” U.S. patent 6486651, Nov. 26, 2002.

[20] Y.k. Ho, H. Chung, S. Lee and S.Y.R. Hui, “A comparative study on dimming control methods for electronic ballasts,” *IEEE Trans. Power Electron.*, Vol 16, pp. 828-836, Nov. 2001.

[21] M. Rico-Secades, E.L. Corominas, J.M. Alonso, J. Ribas, J. Cardesin, A.J. Calleja and J. Garcia-Garcia, "Complete Low-cost Two-stage electronic ballast for 70-W high pressure sodium vapor lamp based on current-mode-controlled buck-boost inverter," *IEEE Transactions on Industry applications*, Vol. 41, No.3, pp. 728-734. May/June 2005.

[22] J.M. Alonso, A. J. Calleja, J. Ribbas, E. Corominas and M. Rico-Secades, "Evaluation of a novel single-stage high-power-factor electronic ballast based on integrated buck half-bridge resonant inverter," in proc. IEEE APEC'00, Vol. 1, pp. 610-616, Feb -2000.

[23] B.P. Divakar, K.W.E. Cheng, "Study of Dimming control methods for HID automotive lamps," *International conference on Power electronics systems and applications* proceedings, 2006, pp. 277-282.

[24] Liu, K.-H.; Lee, F.C.Y., "Zero-voltage switching technique in DC/DC converters", *IEEE Transactions on Power Electronics*, Vol. 5, No. 3, pp. 293 -304, July 1990

[25] K.W.E.Cheng and P.D.Evans, "Unified theory of extended-period quasi-resonant converters", *IEE Proceedings- Elect. Appl.*., Vol. 147, No. 2, , pp. 119-130. March, 2000

[26] R.L.Steigerwald, High frequency resonant transistor DC/DC converters", *IEEE Trans. Power Electronics*, 1E-31 (2), pp. 181-191.

[27] Chan H.L., Cheng K.W.E., and Sutanto D., "Phase-shift controlled DC-DC converter with bi-directional power flow", *IEE Proceedings-Electr. Power Appl.*, Vol. 148, No. 2, pp. 193-201 , March 2001.

[28] K.W.E.Cheng, "Zero-current-switching switched-capacitor converters", *IEE Proceedings-Electr. Power Appl.*, Vol. 148, No. 5, pp. 403-409, Sep 2001.

[29] Y.P.Yeung, K.W.E.Cheng and D.Sutanto, "Investigation of multiple output operation for switched-capacitor resonant converters", *Int. Journal Circuits Theory & App*, Vol. 30, Issue 4, pp. 411-423, Mar 2002.

[30] Y.P.Yeung, K.W.E.Cheng, D.Sutanto, and S.L.Ho, "Zero-current switching switched-capacitor quasi-resonant step-down converter", *IEE Proceedings – Electr. Power Appli*., Vol 149, Issue 02, pp. 111-121 March 2002.

[31] K.K.Law, K.W.E.Cheng and Y.P.B.Yeung, “Design and analysis of switched-capacitor based step-up resonant converters”, *IEEE Trans Circuit Systems I*, Vol.52, Issue 4, April 2005.

[32] K.K. LAW and K.W.E. CHENG, “Examination of the frequency modulation and lifting techniques for the generalized power factor correction switched-capacitor resonant converter”, *International Journal of Circuit Theory and Application*, cta.462, 15 Nov 2007.

[33] M. Zribi and J.Chiasson, “Position control of a PM stepper motor by exact linearization”, IEEE Trans Automatic Control, Vol. 36, No. 5, May 1991, pp. 620-625.

[34] P. Crnosija, B. Kuzmanovic and S. Ajdukovic, “Microcomputer implementation of optimal algorithm for closed-loop control of hybrid stepper motor drives”, IEEE Trans Industrial Electronics, Vol. 47, No. 6, ec 2000, pp. 1319-1325.

Bibliography

[1] T.H. Chen, J.L. Chen, C.H. Chen and C.M. Chang, “Vehicle Detection and Counting by Using Headlight Information in the Dark Environment”, *Third International Conference Intelligent Information Hiding and Multimedia Signal Processing*, 2007. IIHMSP, Vol. 2, pp.519-222, 26-28 Nov. 2007.

[2] J. Berssenbrugge, J. Bauch and J. Gausemeier, “A Night Drive Simulator for the Evaluation of a Predictive Advanced Front Lighting System”, *ITI 4th International Conference Information & Communications Technology*, 2006. ICICT '06., pp. 1-2, Dec. 2006